First-principles calculations of the phase diagrams of noble metals: Cu-Au, Cu-Ag, and Ag-Au

S. -H. Wei, A. A. Mbaye, L. G. Ferreira, and Alex Zunger
Solar Energy Research Institute, Golden, Colorado 80401
(Received 11 May 1987)

It is shown how the temperature-composition phase diagrams and thermodynamic properties of noble-metal alloys can be accurately reproduced by solving the three-dimensional nearest-neighbor fcc Ising model with volume-dependent interaction energies determined from the properties of the ordered phases alone. It is found that lattice relaxation effects are essential in determining order-disorder critical temperatures. This approach enables the understanding of phase diagrams in terms of the electronic properties and atomic-scale structure of the constituent ordered phases.

I. INTRODUCTION

The observed temperature-composition phase diagrams of the face-centered-cubic (fcc) noble-metal alloys[1] (Fig. 1) exhibit many of the qualitative phenomena underlying phase equilibria of alloys: order-disorder transitions and multiple-phase coexistence in Cu-Au [Fig. 1(a)], limited solubilities and a broad miscibility gap in Cu-Ag [Fig. 1(b)], and complete solid solutions in Ag-Au [Fig. 1(c)]. This diversity of phase phenomena, coupled with the relative simplicity of the electronic and crystal structures of the ordered phases of noble-metals compounds are largely responsible for the fact that these systems constituted the testing grounds for nearly all theoretical approaches to phase stability. This includes electronic structure calculations for *distinct ordered phases*,[2-5] empirical models for charge transfer in *ordered phases*,[6,7] coherent potential approaches to the properties of the *homogeneous disordered alloys*,[8-11] tight-binding cluster-Bethe-lattice approaches[12] to the *order-disorder transition* in Cu-Au, and various solutions to the *phase diagram* problem modeled by the three-dimensional spin-$\frac{1}{2}$ fcc Ising model[13,14] and solved approximately by the cluster variation method[15-19] (CVM), Monte Carlo simulations,[20-22] or high-temperature expansions.[23] Despite the fact that the phase diagrams of noble metals are by far both experimentally and theoretically the best studied metallurgical system, with the exception of Ref. 12, no attempt has been made to relate the phase diagram to the *electronic* structure of the constituents. Recently[24-26] we have outlined the way in which the phase diagram of an alloy can be obtained from the volume-dependent total energy of its ordered "building blocks." We will apply this method here to study from first principles the phase diagrams of noble metals.

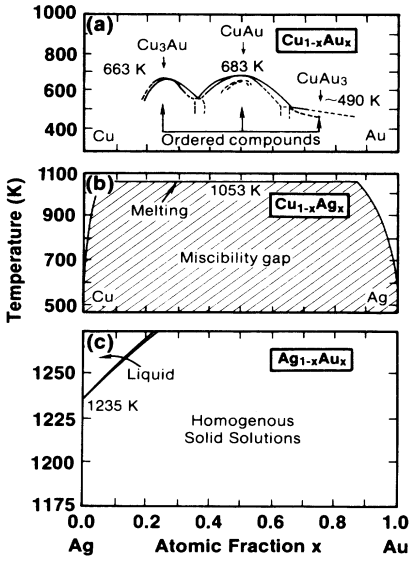

FIG. 1. Experimental (Ref. 1) phase diagrams of noble-metal alloys.

The volume (V) -dependent excess internal energy $\Delta E(\sigma,V)$ of an alloy made of N_A A atoms and N_B B atoms (where $N=N_A+N_B$) in a state of order σ (any of the 2^N possible arrangements on a fixed lattice) is defined with respect to equivalent amounts of the elemental solids A and B as

$$\Delta E(\sigma,V)=E(\sigma,V)-\frac{N_A}{N}E_A(V_A)-\frac{N_B}{N}E_B(V_B)\ , \qquad (1)$$

where $E(\sigma,V)$ is the total energy of the alloy, and $E_A(V_A)$ and $E_B(V_B)$ are the total energies of the constituents at their respective equilibrium volumes V_A and V_B. On each lattice site i, one can have either a B atom (in which case we denote the spin variable as $S^{(i)}=1$ and the occupation variables as $\eta_1^{(i)}=1$ and $\eta_0^{(i)}=0$) or an A atom (in which case the spin variable is $S^{(i)}=-1$ and the occupation variables are $\eta_1^{(i)}=0$ and $\eta_0^{(i)}=1$). This general Ising problem is then often simplified[20] by limiting the interaction to a tractable short range and to a finite number of multisite couplings within this range. For instance, limiting the interaction range to first neighbors and truncating the many-atom couplings to include up to four-body terms, the Hamiltonian can be written as

$$E=J_0N+J_1\sum_{\text{points}}S^{(i)}+J_2\sum_{\text{pairs}}S^{(i)}S^{(j)}+J_3\sum_{\text{triangles}}S^{(i)}S^{(j)}S^{(k)}+J_4\sum_{\text{tetrahedra}}S^{(i)}S^{(j)}S^{(k)}S^{(l)}\ , \tag{2}$$

where the interaction parameters $\{J\}$ can be volume dependent. The Hamiltonian of Eq. (2) can also be written in the form

$$E=\sum_{p,q,r,s}E(p,q,r,s)\frac{1}{N_4}\sum_t\eta_p^{(i)}\eta_q^{(j)}\eta_r^{(k)}\eta_s^{(l)}\ , \tag{3}$$

where t enumerates tetrahedra, N_4 is their number, and $E(p,q,r,s)$ is the energy of a tetrahedron [expressible as linear combinations of the J's of Eq. (2), see Ref. 20] with occupations p,q,r,s (zero or one). Subtracting from $E(p,q,r,s)$ the energies

$$\frac{N_A}{N}E(0,0,0,0)+\frac{N_B}{N}E(1,1,1,1)$$

of equivalent amounts of the pure constituents, defining the multiple index $n=(p,q,r,s)$, and the state-of-order-dependent multisite correlation functions

$$\xi_n(\sigma)=\frac{1}{N_4}\sum_t\eta_p^{(i)}\eta_q^{(j)}\eta_r^{(k)}\eta_s^{(l)}\ , \tag{4}$$

Eq. (3) becomes

$$\Delta E(\sigma,V)=\sum_n\Delta E(n,V)\xi_n(\sigma)\ , \tag{5}$$

where the energy of the alloy at any state of order σ is expressed as a weighted superposition of the energies of its building blocks, with weights $\xi_n(\sigma)$ describing the occurrence frequencies of each building block.

In general the lattice parameter (hence volume) changes with composition. Hence, each of the interaction "parameters" $\Delta E(n,V)$ of Eq. (5) is, in fact volume dependent, i.e., an equation of state at $T=0$ (note that all traditional Ising model approaches[13–21] assume *constant* interaction energies). The physical content of these volume dependent parameters $\Delta E(n,V)$ can be conceptualized in the following way. If all the N_4 tetrahedra have the same occupation numbers n, then Eq. (4) implies that the multisite correlations are

$$\xi_m(n)=\delta_{nm}\ . \tag{6}$$

Conceptualizing such a state of order as a periodic crystal whose repeat unit is this tetrahedron, Eq. (5) lets us interpret the volume-dependent parameters $\Delta E(n,V)$ as the excess energy of the *ordered* structure n. An alloy could then be desired as a collection of all local atomic environments [each occurring in the alloy with the frequency $\xi_n(\sigma)$] exhibited by the corresponding ordered crystals. At any state of order σ of the system (ordered or not), the equilibrium volume $[V_{\text{eq}}(x)]$ is given by the minimum condition

$$\frac{d}{dV}\Delta E(\sigma,V)=\sum_n\xi_n(\sigma)\frac{d}{dV}\Delta E(n,V)=0\ . \tag{7}$$

Considering a (canonical) ensemble of samples of given concentration x, the probability of finding a given unit n becomes a thermal average

$$P_n(x,T)=\langle\xi_n(\sigma)\rangle\ , \tag{8}$$

and the excess enthalpy of mixing at the equilibrium volume V_{eq},

$$\Delta H(x,T)=E[\sigma,V_{\text{eq}}]-xE_A[V_A]-(1-x)E_B[V_B]\ , \tag{9}$$

becomes

$$\Delta H(x,T)=\sum_n\Delta E(n,V_{\text{eq}})P_n(x,T)\ . \tag{10}$$

Our method is then based on the following steps.

(i) Identify a set of ordered structures A_nB_{4-n} which exhibit all the local nearest-neighbor atomic environments characteristic of the A_xB_{1-x} alloy. We use for this purpose the five Landau-Lifshitz[27] ordered fcc structures for the (001) ordering vector, i.e., for $n=0$ and $n=4$ we use the $A1$ fcc structure, for $n=1$ and 3 the $L1_2$ structure, and for $n=2$ the $L1_0$ structure. These crystal structures, their space groups, atomic positions, and lattice vectors are depicted in the first three columns of Fig. 2. The choice of these structures (observed to occur in Cu-Au alloys[1]) implies a nearest-neighbor approximation.

(ii) For each of the five ordered structures A_nB_{4-n}, calculate self-consistently its total energy $E[A_nB_{4-n};V]$ as a function of volume. Use these to obtain the volume-dependent interaction energies per atom $\Delta E(n,V)$ of the *ordered* phases

$$\Delta E(n,V)=\tfrac{1}{4}E[A_nB_{4-n};V]-\frac{n}{4}E_A[V_A]-\frac{4-n}{4}E_B[V_B]\ , \tag{11}$$

appearing in Eqs. (1) and (5).

(iii) With these interaction energies, solve for the correlation functions $\xi_n(\sigma)=\xi_n(x,T)$ appearing in the Ising Hamiltonian [Eqs. (2)–(5)] using, say, the cluster variation method.[15–19]

(iv) Obtain the probabilities $P_n(x,T)$ from Eq. (8), and from these the entropy $S(x,T)$, enthalpy [Eq. (10)], and hence free energies of all possible (ordered or disordered) phases.

(v) Construct the x-T phase diagram from the free energies of all species, using standard thermodynamic methods.[28] The approximations involved in this approach will be discussed in Sec. II C, after the results of the local density calculations (Secs. II A and II B) are introduced.

	B n=0,4 A1 Au type	AB n=2 LI_0 CuAu-I type	A_3B n=1,3 $L1_2$ Cu_3Au type	AB n=1,3 $L1_1$ CuPt type
	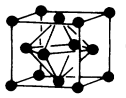	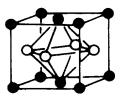	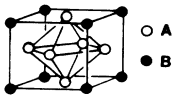	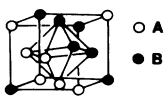
Bravais lattice	Cubic	Tetragonal	Cubic	Rhombohedral (=Trigonal)
Atomic positions	B at (000)	A at (0½½) B at (000)	3A at {(½0½) (0½½); (½½0)} B at (000)	A at (111) B at (000)
Space group	O_h^5 ; $Fm\bar{3}m$; cF4 (225)	D_{4h}^1 ; P4/mmm; tP4 (123)	O_h^1 ; $Pm\bar{3}m$; cP4 (221)	D_{3d}^5 ; $R\bar{3}m$ (166)
Coordination	B: 12 B NN	A: 8B and 4A NN B: 8A and 4B NN	A: 4B and 8A NN B: 12A NN	A = 6B and 6A NN B = 6A and 6B NN
Lattice vectors	$\bar{t}_1$ = (½, ½ 0) a $\bar{t}_2$ = (0, ½, ½) a $\bar{t}_3$ = (½, 0, ½) a	$\bar{t}_1$ = (½, ½, 0) a $\bar{t}_2$ = (-½, ½, 0) a $\bar{t}_3$ = (0, 0, 1) a	$\bar{t}_1$ = (1, 0, 0) a $\bar{t}_2$ = (0, 1, 0) a $\bar{t}_3$ = (0, 0, 1) a	$\bar{t}_1$ = (½, ½, 1) a $\bar{t}_2$ = (1, ½, ½) a $\bar{t}_3$ = (½, 1, ½) a
Equivalent superlattice	None	(1, 1) in (001) direction	None	(1, 1) in (111) direction

FIG. 2. Structural properties of simple fcc-derived ordered phases of the type A_nB_{4-n} for $0 \leq n \leq 4$.

II. FIRST PRINCIPLES TOTAL ENERGY CALCULATIONS FOR THE ORDERED PHASES OF NOBLE METALS

A. Method of the calculation

Band structure and total-energy calculations for ordered A_nB_{4-n} (where A, B are Cu, Ag, or Au) compounds were performed using the all-electron general potential linear augmented-plane-wave (LAPW) method[29] within the local-density-functional formalism,[30] using the Wigner[31] exchange-correlation functional. In this calculation, semirelativistic (i.e., without spin-orbit coupling) effects are included for the valence states, whereas the core states are treated fully relativistically in an atomic-like procedure. The muffin-tin (MT) radii are chosen to be 2.3324 a.u. for Cu and 2.5679 a.u. for Ag and Au. The cutoff kinetic energy for the LAPW basic functions are 11.8 Ry (equivalent to about 70–80 LAPW basis functions per atom) and are kept the same for all calculations. Our cohesive energies are converged to be better than 0.1 eV. No shape approximation is made for either the potential or the charge density. Inside the atomic spheres the nonspherical charge and potential are expanded in terms of lattice harmonics of angular momentum $l \leq 6$.

The Brillouin-zone (BZ) integration for the charge density is performed using a discrete **k**-point summation.

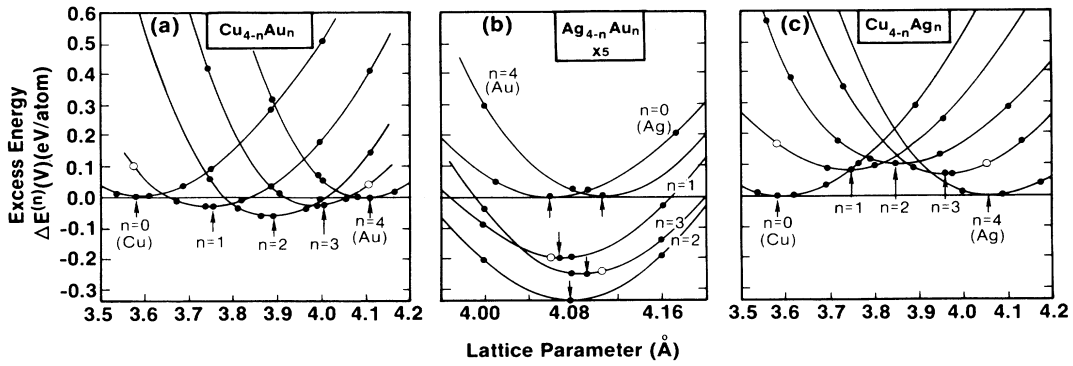

FIG. 3. Lattice parameter-dependent total excess energies (with respect to equivalent amounts of the elemental solids at equilibrium) of noble-metal phases in the fcc structure (Cu, Ag, and Au), $L1_0$ structure ($n=2$) and $L1_2$ structures A_3B ($n=1$) and AB_3 ($n=3$). See Fig. 2 for structural information. The full circles are the calculated points. The empty circles give the calculated limiting partial mixing enthalpies $\Omega_H(0)$ and $\Omega_H(1)$ [Eq. (28) below]. The arrows point to the equilibrium lattice constants.

TABLE I. Comparison of the ground-state properties (lattice parameter, in Å, bulk modulus in GPa, and cohesive energy in eV/atom) of fcc noble metals, as obtained by various computational approaches to the local density formalism.[2,34–38] The present results are obtained in the semirelativistic full-potential linear augmented-plane-wave (LAPW) method, using Wigner's exchange correlation.[31] The augmented-spherical-wave (ASW) method used in Ref. 2 employs a shape-approximated potential, is semirelativistic, and uses the exchange-correlation potential proposed by Moruzzi *et al.*[35] The ASW work of Ref. 34 is nonrelativistic and uses the Hedin-Lundqvist exchange-correlation potential.[36] The ASW calculations of Refs. 2 and 34 differ by 0.05 Å in lattice constant. The mixed-basis (MB) pseudopotential methods of Ref. 37 use a shape unrestricted potential, are nonrelativistic, and use the Ceperley and Alder exchange-correlation potentials as parametrized by Perdew and Zunger.[38] The Korringa-Kohn-Rostocker (KKR) method of Ref. 35 uses a muffin-tin potential, is nonrelativistic, and employs the exchange-correlation potential of Ref. 35.

	Cu	Ag	Au
	Lattice parameter (Å)		
Present, LAPW	3.577	4.057	4.106
ASW[a]	3.554	4.028	4.070
ASW[b]	3.602		
MB[c]	3.625		
KKR[d]	3.581	4.123	
	Bulk modulus (GPa)		
Present, LAPW	144	106	180
ASW[a]	186	137	189
ASW[b]	129		
MB[c]	150		
KKR[d]	152	102	
	Cohesive energy (eV/atom)		
Present, LAPW	4.33	3.53	4.35
ASW[a]			
ASW[b]	4.05		
MB[c]	3.35		
KKR[d]	4.10	2.88	

[a]Reference 2.
[b]Reference 34.
[c]Reference 37.
[d]Reference 35.

For the $A1$ fcc structure ten special **k** points[32] in the irreducible portion of the BZ (64 in the full BZ) are used. To test the convergence of the results with respect to this sampling we calculated the ground-state properties of Cu using 28 **k** points and compared the results obtained using 10 **k** sampling points. We find the lattice constant to increase by only 0.013 Å, the bulk modulus decreases by 8% and cohesive energy increases by 1%. These changes reflect the relative precision of our first principle calculation. For calculating the (generally small) excess energies $\Delta E(n,V)$ [Eq. (11)] of compounds in different crystal structure we have used the *equivalent* **k**-points method to eliminate random errors due to the **k**-point sampling. In this procedure the **k** points in the full BZ of the $A1$ (fcc) structure, used to generate the ten special **k** points for fcc crystal, are mapped into the irreducible portion of the BZ of $L1_0$ (generating 12 **k** points), of $L1_2$ (generating 4 **k** points), and of $L1_1$ (generating 15 **k** points). This mapping guarantees that the total energy per atom of an elemental metal calculated either with the fcc unit cell or with a lower symmetry unit cell (e.g., $L1_0$, $L1_1$, $L1_2$) are *identical*. Finally, each eigenvalue is effectively broadened using an artificial Fermi-Dirac distribution corresponding to a thermal energy of $kT=2$ mRy to improve the convergence of the **k**-space summations.

B. Ground-state properties and heat of formation of the ordered alloy

The calculated total energies as a function of lattice parameters for the A_nB_{4-n} ($n=0,1,2,3,4$) noble-metal compounds are depicted in Fig. 3. These were fitted to the Murnaghan's equation of state[33] to find the equilibrium lattice constants $a_{\rm eq}^{(n)}$, bulk moduli $B^{(n)}$, and the pressure derivatives $B_p^{(n)}$ of the bulk modulus. We have used for this fitting procedure 4–5 values of the lattice parameters near the equilibrium position. Calculated results for fcc Cu, Ag, and Au are given in Table I, where they are compared with the results of previous calculations.[2,34–38] The cohesive energies for the elemental solids are obtained by subtracting the atomic total energies in the $d^{10}s^1$ configuration from the total energies of the solids using the von Barth-Hedin exchange-correlation potential.[39] The spin-polarization energies (with respect to the unpolarized energies) are found to be -0.27, -0.21, and -0.18 eV for the Cu, Ag, and Au atoms, respectively. For the tetragonally-deformed ($\eta=c/a$; $\eta\neq1$) AB compound in the $L1_0$ phase the equilibrium structure is found by searching the minimum of total energy in the two dimension (a,η) plane. After finding the equilibrium positions the bulk modulus is obtained approximately by calculating total energy as function of volume with fixed equilibrium c/a ratio. Our calculated results for the ordered binary compounds are given in Table II and Table III, where they are compared with the results of earlier calculations[2,3] and with experimental data.[40–52]

The dependence of the ground-state properties on exchange-correlation potential has been examined for Cu and Au. We find that using the Hedin-Lundqvist correlation formula[36] the calculated lattice constants for Cu and Au are 3.534 and 4.081 Å, respectively, about 1% smaller than those calculated from Wigner's interpolation formula.[31]

For the Cu-Au and Cu-Ag systems total-energy calculations have been extended to values of lattice parameters covering the full range where alloys form (3.577 Å $< a <$ 4.106 Å, Fig. 3). To minimize the fitting errors near the equilibrium positions, we fixed $a_{\rm eq}^{(n)}$, $B^{(n)}$, and the cohesive energy $E_c^{(n)}$ to the values calculated near equilibrium (Tables I and II), retaining as the only fitting parameter the pressure derivative $B_p^{(n)}$. The resulting fits are used in the phase diagram calculation (see Sec. III

TABLE II. Comparison of the ground-state properties (lattice constant $a_{eq}^{(n)}$, bulk modulus $B^{(n)}$, and formation enthalpy $\Delta H^{(n)}$) of intermetallic compounds of noble metals as obtained by different computational approaches to the local density problem. See caption to Table I for details. The AB and A_3B structures are $L1_0$ and $L1_2$, respectively. T and C refer to tetragonal ($c \neq a$) and cubic ($c = a$), respectively.

	$a_{eq}^{(n)}$ (Å)		$B^{(n)}$ (GPa)		$\Delta H^{(n)}$ (kcal/g-at.)	
System	Present	ASW[a]	Present	ASW[a]	Present	ASW[a]
Cu_3Au	3.738	3.697	140	188	−0.83	−1.50[b]
CuAu	$a = 4.022$					
	$c = 3.630$		162		−1.45(T)	
	$\bar{a} = 3.887$	3.830		191	−1.21(C)	−1.61
$CuAu_3$	3.991	3.955	194	186	−0.61	−0.78
Ag_3Au	4.068	4.034	125	151	−0.98	−1.02
AgAu	$a = 4.057$					
	$c = 4.122$		142		−1.56(T)	
	$\bar{a} = 4.079$	4.043		168	−1.55(C)	−1.39
$AgAu_3$	4.093	4.056	164	175	−1.16	−1.05
Cu_3Ag	3.731	3.677	137	172	+1.78	+1.98
CuAg	$a = 3.966$					
	$c = 3.622$		115		+2.34(T)	
	$\bar{a} = 3.848$	3.795		161	+2.39(C)	+2.73
$CuAg_3$	3.963	3.914	155	146	+1.58	+2.10

[a]Reference 2.
[b]Reference 3 obtained $\Delta H(Cu_3Au) = -1.18$ kcal/g-at.

and Table VI). The fitting error is about 10^{-2} mRy for points near the equilibrium positions, and about a few mRy for points far away from the equilibrium positions.

The heat of formation per atom $\Delta H^{(n)}$ of the ordered compounds from the elemental solids is defined as the equilibrium value of $\Delta E(n, V)$ of Eq. (11), i.e.,

$$\Delta H^{(n)} \equiv \Delta E(n, V_{eq}) = \tfrac{1}{4} E[A_n B_{4-n}; V_{eq}] - \frac{n}{4} E_A[V_A] - \frac{4-n}{4} E_B[V_B] . \quad (12)$$

By definition, the formation enthalpies of the end-point constituents ($n = 0, 4$) are zero. A negative heat of formation indicates the compound to be stabler then its end-point constituents. The significance of negative/positive formation enthalpies in terms of the electronic structure is discussed in Sec. II D.

C. Basic approximations

Our approach to the alloy phase diagram problem involves three basic approximations.

(i) Even if five basic stoichiometric structures (Fig. 2) were sufficient to describe the properties of the alloy at all compositions, the local density approximation provides but an imperfect description of the ground-state properties of these five structures relative to experiment (Table III). We will examine the consequences of these errors on the phase diagrams in Sec. IV ("model B"), where the *experimental* values of $\{a_{eq}^{(n)}, B^{(n)}, \Delta H^{(n)}\}$ would be used instead of the local density values ("model A"). The sensitivity of the phase diagrams to small changes of $\{a_{eq}^{(n)}, B^{(n)}, \Delta H^{(n)}\}$ will be further examined in Sec. V ("model C").

(ii) The actual alloy may exhibit lattice relaxation effects,[53] (equivalent to using a very large number of ordered building blocks, differing from one another by small distortions), whereas we have implied so far the use of *unrelaxed* structures. We will introduce such relaxation effects in Sec. VI ("model D").

(iii) Each of the ordered structure used includes but a *single type* of tetrahedron, e.g., the A_4 and B_4 tetrahedra in the $A1$ phases ($n = 0$ and $n = 4$, respectively), the A_2B_2 tetrahedron in the $L1_0$ phase ($n = 2$), and the AB_3 ($n = 1$) and A_3B ($n = 3$) tetrahedra in $L1_2$ phase. Our

TABLE III. Calculated LAPW and experimental ground-state properties (lattice constant $a_{eq}^{(n)}$, bulk modulus $B^{(n)}$, cohesive energy $E_c^{(n)}$, formation ethalpy $\Delta H^{(n)}$, and pressure coefficient $B_p^{(n)}$ of the bulk modulus) of the fcc noble metals and their ordered compounds AB ($L1_0$ structure) and A_3B, AB_3 ($L1_2$ structure). The calculation uses the semirelativistic local density-functional approach with the Wigner exchange correlation. $\bar{a}$ is the cubic lattice constant giving equivalent volume to that of the tetragonal ($c/a \neq 1$) structure. Keeping cubic symmetry ($c=a$) for CuAu gives $a_{cubic}=3.880$ Å. Also given are the decomposition of $\Delta H^{(n)}$ to a "chemical" part $\varepsilon^{(n)}$ and an "elastic" part $G(X_n)$ [see Eqs. (18)–(22)].

	$a_{eq}^{(n)}$ (Å)		$B^{(n)}$ (GPa)		$E_c^{(n)}$ (eV/atom)		$\Delta H^{(n)}$ (kcal/g-at.)		$B_p^{(n)}$		$\varepsilon^{(n)}$ (kcal/g-at.)		$G(X_n)$ (kcal/g-at.)	
System	Calc.	Exptl.	Calc.	Exptl.	Calc.	Exptl.	Calc.	Exptl.	Calc.	Exptl.	Calc.	Exptl.	Calc.	Exptl.
Cu	3.577	3.615[a]	144	138[b]	4.33	3.49[c]	0.0	0.0	5.6	5.4[d]	0.0	0.0	0.0	0.0
Ag	4.057	4.086[e]	106	102[f]	3.53	2.95[c]	0.0	0.0	5.8	6.1[g]	0.0	0.0	0.0	0.0
Au	4.106	4.078[h]	180	171[f]	4.35	3.81[c]	0.0	0.0	5.2	6.1[i]	0.0	0.0	0.0	0.0
Cu_3Au	3.738	3.743[j]	140	148[k]	4.37	3.64[l]	−0.83	−1.71[m]	7.2		−6.49	−5.93	5.66	4.22
CuAu	$a=4.022$ $c=3.630$ $a=3.887$	$a=3.966$[n] $c=3.673$ 3.876[o]	162	163[p]	4.40	3.74[l]	−1.45	−2.10[m]	8.6		−8.22	−7.72	6.77	5.62
$CuAu_3$	3.991	3.982[q]	194	170[r]	4.37	3.79[l]	−0.61	−1.37[s]	4.3		−5.28	−5.45	4.67	4.08
Ag_3Au	4.068		125		3.78		−0.98		5.7		−1.02		0.04	
AgAu	$a=4.057$ $c=4.122$ $a=4.079$		142		4.01		−1.56		5.5		−1.62		0.06	
$AgAu_3$	4.093		164		4.20		−1.16		5.4		−1.21		0.05	

TABLE III. (*Continued*).

System	$a_{eq}^{(n)}$ (Å) Calc.	Exptl.	$B^{(n)}$ (GPa) Calc.	Exptl.	$E_c^{(n)}$ (eV/atom) Calc.	Exptl.	$\Delta H^{(n)}$ (kcal/g-at.) Calc.	Exptl.	$B_p^{(n)}$ Calc.	Exptl.	$\varepsilon^{(n)}$ (kcal/g-at.) Calc.	Exptl.	$G(X_n)$ (kcal/g-at.) Calc.	Exptl.
Cu_3Ag	3.731		137		4.05		+1.78		4.9		−1.92		3.70	
CuAg	$a=3.966$ $c=3.662$ $a=3.848$		115		3.83		+2.34		5.8		−2.23		4.57	
$CuAg_3$	3.963		155		3.66		+1.58		4.1		−1.84		3.42	

[a]Room temperature, Ref. 40.
[b]Reference 41.
[c]Reference 42.
[d]From the pressure coefficient of the elastic constants at low pressure, Ref. 43.
[e]Room temperature, Ref. 44.
[f]Reference 45.
[g]From the pressure coefficients of the elastic constants at low pressure, see Ref. 46.
[h]Room temperature, Ref. 47.
[i]From the pressure coefficients of the elastic constants at low pressure, Ref. 48.
[j]Room temperature, Ref. 49.
[k]Reference 50.
[l]Calculated from the experimental cohesive energy of the elemental solids (Ref. 42) and $\Delta H^{(n)}$ (Ref. 1).
[m]Reference 1, Table 1b, p. 262 and Table 3, p. 264.
[n]Room temperature, Ref. 51.
[o]This is the value for the disordered phase at room temperature given in Ref. 51.
[p]For the cubic phase, Ref. 50.
[q]Room temperature, Ref. 52.
[r]Obtained by interpolating the bulk moduli at other Au concentrations, see Refs. 41, 49, and 51.
[s]This is our estimate based on the differences of heat of formation at $T=800$ K for Cu_3Au, and Au_3Cu given in Ref. 1, Table 4, p. 264. The expected error in this estimate is a few tenths of a kcal/g-at.

nearest-neighbor approach hence implies that the energy $\Delta E(\sigma,V)$ of structures with an arbitrary arrangement of tetrahedra (including, for example, cases where two different tetrahedra such as A_3B-AB_3 coexist in the same cell) can be approximately described by a superposition of the energies $\{\Delta E(n,V)\}$ of periodic structures, each containing a *single type* of tetrahedron. The adequacy of this nearest-neighbor "superposition approximation" is examined as follows: We have calculated the total energy of CuAu and AgAu in the $L1_1$ CuPt structure [space group D^5_{3d}, equivalent to an (1,1) superlattice along the (111) direction, see last column of Fig. 2], a phase which includes *both* A_3B and AB_3 clusters in the same cell. We then compared its excess energy to the average excess energies of the two $L1_2$ structures, each containing only a A_3B or a AB_3 tetrahedron. The nonadditivity $\Delta(a)$ of the excess energies as a function of lattice constant is defined as

$$\Delta(a)\equiv\tfrac{1}{4}\{\Delta E^{(1,3)}_{L1_1}[\tfrac{1}{2}A_3B+AB_3),a]-\tfrac{1}{2}[\Delta E^{(1)}_{L1_2}(A_3B,a)+\Delta E^{(3)}_{L1_2}(AB_3,a)]\}\ , \quad (13)$$

where the $L1_1$ structure is kept cubic (i.e., no structural relaxation). $\Delta(a)$ is hence a measure of the strength and volume dependence of intertetrahedra (*next*-nearest-neighbor) interactions. For the Ag-Au system we find that $\Delta(a)$ is positive ($+0.25$ kcal/g-at.) and nearly a-independent. For the Cu-Au system we also find at $a=3.864$ Å (a value near the equilibrium lattice parameter of CuAu, see Table II) a positive $\Delta(a)=+0.24$ kcal/g-at. Hence, as is the case for the Ag-Au, the $L1_1$ structure of CuAu near equilibrium is also *less* stable than the average of the two $L1_2$ structures. However, at $a=4.080$ Å (a value close to the equilibrium lattice parameter of Au, see Table I) we find for Cu-Au a *negative* value $\Delta(a)=-0.57$ kcal/g-at. (the $L1_1$ system being more stable). These results can be understood qualitatively as follows: Model harmonically the lattice-parameter variation of the energy of the $L1_1$ structure as

$$\Delta E^{(1,3)}_{L1_1}(a)\cong K_{AB}(a-a_{AB})^2+\Delta H^{(1,3)}\ , \quad (14)$$

where K_{AB} is an effective force constant, a_{AB} is the equilibrium lattice constant of the $L1_1$ structure (close to that of the CuAuI structure), and $\Delta H^{(1,3)}$ is its formation enthalpy. Similarly, model the lattice-parameter variation of the average energy of A_3B and AB_3 [second bracketed term in Eq. (13)] as

$$\Delta\bar{E}(a)=\bar{k}(a-\mathbf{a}_{AB})^2+\Delta\bar{H}\ , \quad (15)$$

when $\bar{a}_{AB}$ and $\bar{K}$ are the average lattice constants and force constant, respectively, and $\Delta\bar{H}=[\Delta E^{(1)}(a_{AB})+\Delta E^{(3)}(a_{AB})]/2$. The nonadditivity $\Delta(a)$ of the excess energies would then be

$$\Delta(a)=K_{AB}(a-a_{AB})^2-\bar{K}(a-\bar{a}_{AB})^2+(\Delta H^{(1,3)}-\Delta\bar{H})\ . \quad (16a)$$

For the Ag-Au system the lattice parameters of all ordered compounds are similar (e.g., Ag_3Au, AgAu and $AgAu_3$, see Table III), hence $a_{AB}\cong\bar{a}_{AB}$. For the Cu-Au system the average lattice parameter of Cu_3Au (3.738 Å) and $CuAu_3$ (3.991 Å) is (3.864 Å) close to that of CuAu (3.880 Å) in either the $L1_0$ or the $L1_1$ phases, hence $a_{AB}\cong\bar{a}_{AB}$ too. Consequently,

$$\Delta(a)\cong(K_{AB}-\bar{K})(a-a_{AB})^2+(\Delta H^{(1,3)}-\Delta\bar{H})\ . \quad (16b)$$

Finding for Ag-Au (all a's) that $\Delta(a)=+0.25$ kcal/g-at. and for Cu-Au at $a=a_{AB}\cong3.864$ Å also $\Delta(a_{AB})=+0.24$ kcal/g-at. we conclude that relative to the isolated tetrahedra the two A_3B and AB_3 tetrahedra repel each other by $[\Delta H^{(1,3)}-\Delta\bar{H}]>0$. However, for Cu-Au at the lattice parameter of $a=4.080$ Å which is far from equilibrium we find a *negative* $\Delta(a)=-0.57$ kcal/g-at. Since $[\Delta H^{(1,3)}-\Delta\bar{H}]>0$, this shows that the first term on the right-hand side of Eq. (16b) must be negative, or that $K_{AB}<\bar{K}$. This shows that the *coexistence of two kinds of tetrahedra in the same cell softens the elastic constants (K_{AB}) relative to those ($\bar{K}$) of the structures with isolated tetrahedra.* This softening then reduces the elastic energy of the CuPt $L1_1$ structure by $-0.57-0.24=-0.81$ kcal/g-at. at $a=4.080$ Å. This suggests to us that such a modification of the properties of a given type of tetrahedron due to the existence of other tetrahedron around it (to be referred to below as "relaxation of cell-internal degrees of freedom") can be a viable mechanism of phase stabilization. [Notice that we have assumed a *cubic* $L1_1$ structure, whereas this structure can relax along the (111) direction, further lowering its energy. Our results above are hence upper limits of $\Delta(a)$]. This observation motivated us to investigate the consequences of relaxation on the phase diagrams (our "model D" Sec. VI).

D. Electronic structure and its relation to the cohesive properties

1. Elemental solids

To understand the trends and gain some insight into the stability of noble metals and their alloys we have studied their electronic properties. We find that many of the trends obtained in the total-energy calculations could be rationalized by considering the atomic properties. Table IV shows the calculated atomic s and d valence orbital energies (both semirelativistic and nonrelativistic)

TABLE IV. Local density atomic eigenvalues ε (in eV) and orbital moment $\langle R\rangle$ (in a.u.) of Cu, Ag, and Au calculated with the Hedin-Lundqvist exchange-correlation potential. The nonrelativistic (NR) and semirelativistic (SR) values of the outermost valence s and d states are given.

	$-\varepsilon_s$	$\langle R_s\rangle$	$-\varepsilon_d$	$\langle R_d\rangle$
Cu (NR)	4.77	2.95	5.57	1.04
Cu (SR)	4.95	2.89	5.39	1.05
Ag (NR)	4.37	3.27	8.19	1.40
Ag (SR)	4.81	3.11	7.73	1.42
Au (NR)	4.51	3.31	8.35	1.58
Au (SR)	6.16	2.84	7.14	1.62

for Cu, Ag, and Au. The relativistic energy shifts are large for Au: They deepen (i.e., increase the binding of) the Au 6*s* energy level by 1.65 eV; as this orbital becomes more tightly bound, it in turn better screens the core potential and hence pushes the Au 5*d* orbital energy to a *higher* energy (by 1.21 eV). These relativistic shifts of atomic eigenvalues have the following effects on the cohesive properties.

(i) They localize the *s* orbitals and delocalize the *d* orbitals causing thereby lattice contraction.[54] This explains why Au has a smaller lattice constant than one would expect from a nonrelativistic model (where atoms with a larger atomic number generally have larger lattice constants). The reduction in lattice constant of Au also implies a larger bulk modulus.

(ii) Relativistic effects *reduce* the *s*-*d* energy difference, increase the overlap of *s* and *d* orbitals (Table IV), and therefore enhance the *s*-*d* hybridization. Since for elemental noble metals the *s*-*d* hybridization contributes significantly to the cohesive energy,[55] the relativistic shift also implies an increased cohesive energy for Au. This also explains why Ag has the smallest cohesive energy among the noble metals. As we can see from Table IV, the Ag 4*d* level has the largest binding energy in the series and is fairly localized. This reduces both the *s*-*d* hybridization and the *d* band covalent contribution to cohesion in Ag (See Table I). We have performed a nonrelativistic (NR) total-energy calculation for metallic Au. We find that the lattice constant ($a_{\mathrm{Au}}^{\mathrm{NR}}=4.304$ Å) *increases* by 4.8%, the bulk modulus ($B_{\mathrm{Au}}^{\mathrm{NR}}=111$ GPa) decreases by -38% and the cohesive energy ($E_c^{\mathrm{NR}}=3.33$ eV) decreases by -23% (Table I). These results substantiate our conclusions.

2. Noble-metal compounds

Our results of Table III indicate that among the noble-metal compounds Cu-Au and Ag-Au are "stable" (negative formation enthalpy), but Cu-Ag is "unstable." Miedema and coworkers[56] have proposed a successful empirical formula to predict the sign of the heat of formation for binary alloys. In their formula the formation of an intermetallic alloy from its constituent solids is associated with two competing contributions to ΔH, represented as

$$\Delta H=-(\Delta\phi)^2+(\Delta\eta)^2 \ . \tag{17}$$

Here, $(\Delta\phi)^2$ is the attractive term related to the electronegativity difference, or the ability to attract electrons, whereas $(\Delta\eta)^2$ is a repulsive term related to the discontinuity of electron density at the boundary of atomic cell of the pure metals. The efforts[7,57–61] undertaken in the past to understand the microscopic origin of the attractive and repulsive terms of Eq. (17) can be broadly divided into two conceptually different models. (i) The ionic model,[7] in which the alloy formation is thought to be *inhibited* by the strain energy (required to fit two lattice mismatched elemental solids in the same alloy), and is *favored* by the charge flow induced by the different chemical potentials of the constituents. (ii) The covalent model[58,59] in which the *s* and *p* electrons, which are responsible for the charge arrangement, are ignored; the attractive contribution to ΔH in this model is then ascribed to the enhancement of interatomic covalent bonds due to the broadening of the *d* bands of the constituents, whereas the repulsive contribution is thought to originate from the mismatch of the widths of the constituents *d* bands.

We find that neither the ionic model nor the covalent model provide a satisfactory and complete picture of the formation of the noble metal alloys. For example, conventional electronegativity scales used in the ionic model often predict an incorrect *direction* of charge transfer. Using, for example, Pauling's scale[62] (where the electronegativities of Cu, Ag, and Au are 1.9, 1.9, and 2.4, respectively) suggests that the charge transfer in the Ag-Au system is from Ag to Au. We find, however, (see Table V) that the actual charge transfer is from Au to Ag, i.e., in the opposite direction. In Table V we see also that the direction of charge transfer is *l* dependent: the *s* and *d* channels always transfer charge in opposite direction.[61] The change of charge density on the nucleus is found to be correlated to the *s* charge transfer. This suggests that the assignment[7] of a single, *l*-independent chemical potential (or electronegativity) is not appropriate. The covalent model also cannot explain some of the results we found. For example, the calculated *d*-band widths [defined as $W_d=\varepsilon(X_5)-\varepsilon(X_1)$] are 3.46, 3.76, and 5.57 eV for Cu, Ag, and Au, respectively. Since the band width mismatch for CuAu is larger than that of CuAg, the covalent model[58] would suggest that CuAg is more stable than CuAu, a conclusion which is not supported by our total-energy calculation or by experiment (Table III). Further, since in the covalent model[58] the nominal *d* occupation number of noble metal is ten, this model would suggest that the *d*-band contribution to bonding is zero, which is inappropriate.

3. Separation of the formation enthalpies into "chemical" and "elastic" contributions

A qualitative understanding of the phase stability problem has been developed recently by approximately separating[26] the excess energy $\Delta E(\sigma,V)$ of an alloy in a state of order σ into a volume-independent but configuration (n)-dependent "chemical energy" $\varepsilon^{(n)}$ and a volume and concentration dependent "elastic energy" $g(x,V)$:

$$\Delta E(\sigma,V)=\sum_n \varepsilon^{(n)}\xi_n(\sigma)+g(x,V) \ . \tag{18}$$

The need for such a separation becomes clear when one realizes[26] that whereas the formation enthalpy $\Delta H^{(n)}=\Delta E(n,V_{\mathrm{eq}})$ of a compound [Eq. (12)] reflects the *balance* between "chemical" and "elastic" energies, the transformation between an ordered compound and a disordered phase of the same composition (e.g., $AB\leftrightarrow A_{0.5}B_{0.5}$, or $A_3B\leftrightarrow A_{0.75}B_{0.25}$) depends solely on $\varepsilon^{(n)}$, since $g(x,V)$ has the same value for ordered and disordered phases at the same composition x and volume. The fact that such a separation is in general nonunique has led in the past to conflicting (and indeed, confusing) models, largely because it was not generally appreciated that one needs to choose a well-defined con-

TABLE V. Site and angular momentum projected charge inside the muffin-tin spheres of Cu ($R_{MT}=2.3324$ a.u.), Ag and Au ($R_{MT}=2.5676$ a.u.), and the charge density differences at the nucleus sites (in e/a.u.^{3}) with respect to the elements.

		Cu site			Ag site			Au site	
	Cu	CuAg	CuAu	Ag	CuAg	AgAu	Au	CuAu	AgAu
s	0.496	0.456	0.427	0.447	0.489	0.421	0.552	0.632	0.585
p	0.413	0.318	0.347	0.310	0.411	0.324	0.357	0.453	0.340
d	9.229	9.270	9.290	9.140	9.106	9.166	8.702	8.636	8.668
$l>2$	0.029	0.021	0.029	0.034	0.050	0.045	0.054	0.067	0.044
Total	10.167	10.061	10.093	9.931	10.056	9.956	9.665	9.788	9.637
$\Delta\rho^o$	0.0	−0.77	−1.40	0.0	2.08	−1.04	0.0	23.9	12.55

straint to make such a separation "unique." Ferreira *et al.*[26] have indeed shown that a rigorous separation is possible if one imposes the reasonable constraint that molar volumes of different phases at the same composition (e.g., ordered *vs* disordered) have but a weak dependence on the state of order. Under this constraint, it was proven that at the equilibrium volume, $g(x,V_{eq})=G(x)$, where

$$G(x)=(1-x)\int_0^x XZ(X)dX+x\int_x^1(1-X)Z(X)dX \ , \quad (19)$$

and

$$Z(x)=\frac{B(x)}{V(x)}\left[\frac{dV}{dx}\right]^2\equiv-\frac{d^2G}{dx^2} \ , \quad (20)$$

and where $B(x)$ and $V(x)$ are the bulk modulus and volume of the alloy, respectively. The excess energy of Eq. (5) for a general state of order σ then becomes

$$\Delta E(\sigma)=\sum_n \varepsilon^{(n)}\xi_n(\sigma)+G(x) \ . \quad (21)$$

For a pure stoichiometric compound all $\xi_n(\sigma)$ but one vanish, giving at equilibrium

$$\Delta H^{(n)}=\Delta E(n,V_{eq})=\varepsilon^{(n)}+G(X_n) \ , \quad (22)$$

where X_n is the concentration of a given atom in the stoichiometric compound (e.g., $X_n=n/4$ for A_nB_{4-n}). The physical interpretation of Eq. (22) is as follows: The first term on the right-hand side represents the formation enthalpy of a compound whose volume $V_{eq}^{(n)}$ equals that of its constituents (V_A and V_B), i.e., for the uncommon case of a lattice-matched alloy. These configuration-dependent (but volume and composition independent) "chemical energies" $\varepsilon^{(n)}$ are then simply the familiar Ising-type "spin-flip" substitution energies[13–21] on this fixed lattice. They measure the strength of the many-body interactions between atoms (or spins) within the interaction range considered. The only reason that the first term of Eq. (21) changes with composition is *statistical:* different alloy compositions have different distributions of species n [given by $\xi_n(\sigma)$], but $\varepsilon^{(n)}$ itself is composition independent.

The second term of Eq. (22) represents corrections to the constant-volume assumption. It vanishes by Eqs. (19) and (20) when the alloy has the same volume as its constituents, i.e., when $dV/dx\equiv 0$, or when the alloy is infinitely compressible $B(x)=0$. The two terms in Eqs. (21) and (22) reflect the dual coordinates used in phenomenological models of solid solubility, compound stability, and mixing enthalpies: The second term can be thought to describe the destabilizing effect of strain induced by the mismatch between the molar volumes of the constituents, and parallels the classical "size factor" in alloy models,[1–4] whereas the first term can be thought to describe the "electronegativity factor."

Using our calculated $\{a_{eq}^{(n)},B^{(n)},\Delta H^{(n)}\}$ values for the noble-metal compounds A_nB_{4-n} (Table III) one can evaluate the two terms of Eq. (22). This is done by evaluating $B(x)$ and $V(x)$ as an interpolation of the values of $B^{(n)}$ and $V^{(n)}$ for five ordered compounds, and integrating Eqs. (19) and (20) to find $G(x)$. Evaluating this $G(x)$ at the stoichiometric compositions $X_n=\frac{1}{4}$, $\frac{1}{2}$, and $\frac{3}{4}$ then gives $G(X_n)$; combined with Eq. (22) and the calculated values of $\Delta H^{(n)}$ (Table III) one then gets all $\varepsilon^{(n)}$'s. For the Cu-Au systems for which sufficient experimental data for ordered compounds exist (Table III) the same procedure can be repeated using the *observed* values of $\{V^{(n)},B^{(n)},\Delta H^{(n)}\}$, resulting in "experimental" values for $\varepsilon^{(n)}$ and $G(X_n)$. These values are given in the last two columns of Table III.

The results point to the following conclusions.

(i) Although Cu-Au and Ag-Au have *negative* $\Delta H^{(n)}$ values but Cu-Ag has *positive* $\Delta H^{(n)}$ values, all three systems have attractive chemical energies $\varepsilon^{(n)}<0$.

(ii) The Cu-Au system has the largest negative chemical energy mainly due to the ability of Au to attract s electrons from other atoms, forming "ionic" bonds, and its ability to give up d electrons, forming "covalent" bonds (Table V). Although the elastic energy $G(X_n)$ of Cu-Au is even larger than that of Cu-Ag (since Au has larger bulk modulus than Ag), the large chemical interactions in Cu-Au overwhelm the destabilizing elastic energy and make this system stable.

(iii) The Cu-Ag system has rather small chemical energies. This can be traced back to the similar s electron levels of its constituents (Table IV) leading to a small ionic charge transfer (Table V), and to the deep d electron energy of Ag (Table IV) depriving the system from significant d-d bonding. The reason that the formation enthalpy $\Delta H^{(n)}$ for Cu-Ag is positive is that its small chemical energy $\varepsilon^{(n)}$ is overwhelmed by the large elastic energy $G(X_n)$ caused by the large lattice mismatch. This large elastic energy will therefore lead to limited solubility *despite* the fact that the chemical energies in Cu-Ag are more attractive than in Ag-Au.

(iv) The Ag-Au system has a negligible elastic energy due to the good lattice match between the constituents (a consequence of relativistic effects, see discussion in Sec. II D 1). Hence, the small chemical energy dominates $\Delta H^{(n)}$ which is therefore negative. The small elastic energy will lead to the formation of complete solid solutions.

(v) Because of the fact that the chemical energy is negative in all three systems, we will find (Sec. III) that Ag-Au has *stable* low-temperature ordered phases (yet unobserved) and that despite $\Delta H(\mathrm{Cu}_n\mathrm{Ag}_{4-n})>0$, the fact that $\varepsilon(\mathrm{Cu}_n\mathrm{Ag}_{4-n})<0$ will lead to *metastable* low-temperature ordered phases in Cu-Ag.

III. MODEL A: CALCULATING THE PHASE DIAGRAMS FROM FIRST PRINCIPLES TOTAL ENERGIES OF UNRELAXED STRUCTURES

Our first step in the study of the phase diagrams of noble metals is to use the five equations of state (described in Table VI as "model A") of the unrelaxed ordered A_nB_{4-n} compounds (Fig. 2) and solve with these interaction energies $\Delta E(n,V)$ (Fig. 3) the three-dimensional nearest-neighbor fcc Ising model [Eqs. (2)–(5)] in the tetrahedron approximation (i.e., retaining up to four body interactions). We use for this purpose the cluster variation method (CVM, see Refs. 15–19). We minimize the free energy not only with respect to the correlation functions $\xi_n(\sigma)$, but also with respect to the volume, obtaining thereby the predicted (generally, non-Vegard-type) composition-dependent volumes. In comparing order-disorder temperatures calculated in the CVM with experiment one must notice that the CVM provides an imperfect solution to the corresponding Ising Hamiltonian: More exact Monte Carlo (MC) simulations of the same Hamiltonian provide slightly lower critical temperatures. In particular, $T_{\mathrm{MC}}/T_{\mathrm{CVM}} \equiv \eta = 0.9425$ for the nearest-neighbor fcc Ising model.[19,20,26] We hence must multiply the calculated critical temperatures by η when comparing with the observed values.

Our calculated phase diagrams in model A are given in Fig. 4 (Cu-Au), Fig. 5(a) (Cu-Ag), and Fig. 6 (Ag-Au). Comparison with the experimental phase diagram (Fig. 1) shows that the *qualitative* features are correctly predicted, e.g., ordered compounds for Cu-Au, a broad miscibility gap for Cu-Ag and complete solubility below melting for Ag-Au. We predict for Cu-Ag [Fig. 5(a)] that inside the miscibility gap there should exist three *metastably ordered* compounds (i.e., with free energies lower than the disordered phase but higher than the two-phase mixture) since $\varepsilon^{(n)}<0$ but $\Delta H^{(n)}>0$. For

TABLE VI. Structural and thermodynamic properties of ordered $\mathrm{Cu}_n\mathrm{Au}_{4-n}$ compounds used in the calculation of the phase diagrams. $a^{(n)}$ in Å, $B^{(n)}$ in GPa, $\Delta H^{(n)}$ in kcal/g-at. An asterisk denotes adjusted quantities.

Quantity	Model A first principle	Model B LT experimental input[a]	Model C adjusted LT experimental input	Model D LT experimental input + relaxation[d]
$a^{(0)}$	3.577	3.615	3.657*	Eq. (24)[d]
$a^{(1)}$	3.738	3.743	3.758*	Eq. (24)[d]
$a^{(2)}$	3.887	3.866	3.852*	Eq. (24)[d]
$a^{(3)}$	3.991	3.982	3.943*	Eq. (24)[d]
$a^{(4)}$	4.106	4.078	4.031*	Eq. (24)[d]
$B^{(0)}$	144	138	138	138
$B^{(1)}$	140	148	148	148
$B^{(2)}$	162	163	163	163
$B^{(3)}$	194	170[b]	170[b]	170[b]
$B^{(4)}$	180	171	171	171
$B_p^{(0)}$	2.92[c]	2.92[c]	2.92[c]	2.92[c]
$B_p^{(1)}$	2.38[c]	2.38[c]	2.38[c]	2.38[c]
$B_p^{(2)}$	6.26[c]	6.26[c]	6.26[c]	6.26[c]
$B_p^{(3)}$	4.82[c]	4.82[c]	4.82[c]	4.82[c]
$B_p^{(4)}$	4.89[c]	4.89[c]	4.89[c]	4.89[c]
$\Delta H^{(1)}$	−0.83	−1.71	−1.59*	−1.556*
$\Delta H^{(2)}$	−1.21[e]	−2.10	−2.100	−2.100
$\Delta H^{(3)}$	−0.61	−1.37[b]	−1.250*	−1.373*

[a]See columns 3, 5, and 9 in Table III for sources of data.
[b]Not measured; interpolated from other data. (See Table III).
[c]Taken from first-principle calculations, model A.
[d]Relaxation parameter $K=0.20772$ in Eq. (24), see text of Sec. VI.
[e]This is the data for cubic CuAuI ($c/a=1$), which is used to calculate the phase diagram. After the relaxation of c/a we find $\Delta H^{(2)}=-1.45$ kcal/g-at.

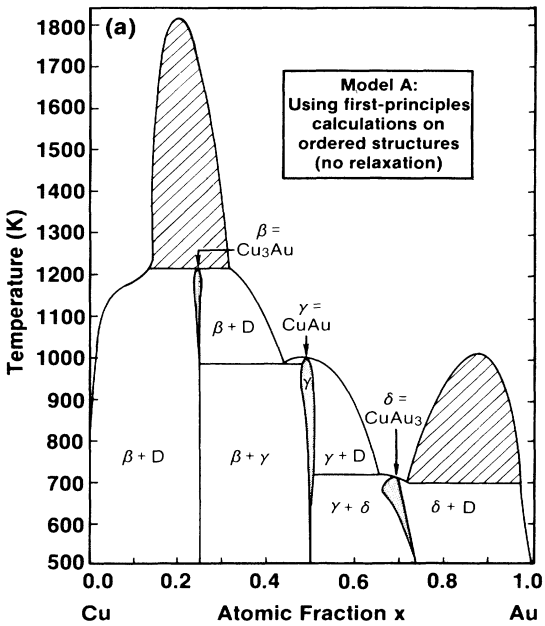

FIG. 4. Calculated phase diagram of Cu-Au using the unrelaxed structural parameters of the ordered building blocks obtained from first-principles calculations (Table VI). Dashed areas denote miscibility gaps, shaded areas denote ordered phases.

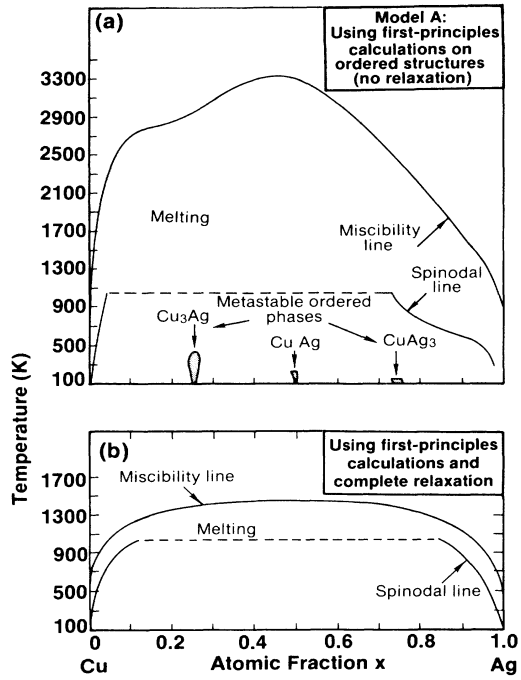

FIG. 5. Calculated phase diagram of Cu-Ag using (a) first-principles calculated structural parameters of the unrelaxed ordered phases (Table III), and (b) fully relaxed ordered phases. Shaded areas denote metastable long-range ordered phases. The boundaries of the metastable phases were defined from $d^2F/dx^2=0$, where F is the free energy of the ordered phase.

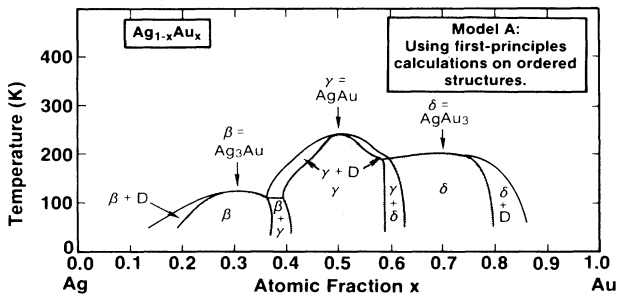

FIG. 6. Calculated phase diagram of Ag-Au using the unrelaxed structural parameters of the ordered building blocks obtained from first-principles calculations (Table III).

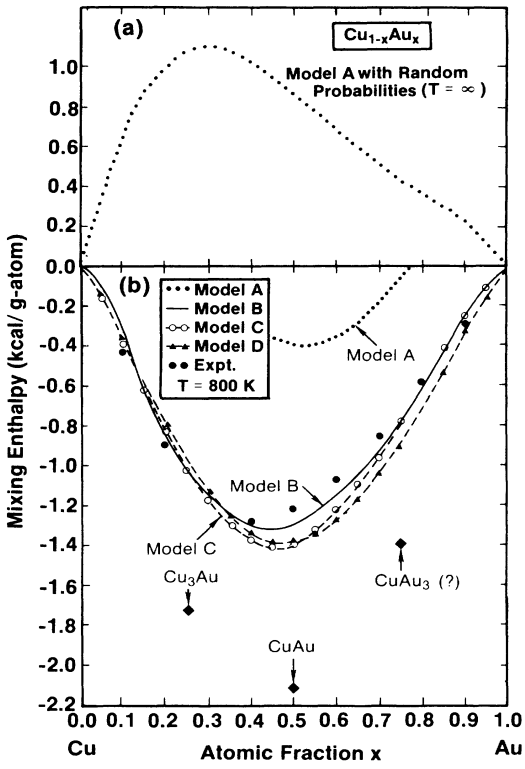

FIG. 7. Calculated excess mixing enthalpies for Cu-Au. (a) Model A but with random probabilities. Observe that the mixing enthalpies are positive in this case, (b) using the actual CVM probabilities for $T=800$ K. Observe that models B, C, and D fit the experimental data closely. Diamond-shaped symbols given the formation enthalpies of the *ordered* phases (the value[1] for $CuAu_3$ is uncertain). The difference between the formation enthalpies and the mixing enthalpies gives the ordering energies [Eq. (29)].

TABLE VII. Predicted critical temperatures T_n (in K) for order-disorder transitions in $Cu_nAu_{4-n} \rightleftarrows Cu_xAu_{1-x}$, miscibility gap (MG) temperature, T_{MG}, mixing enthalpies $\Delta H(X_n, T=800)$, and critical compositions X_n for order-disorder transitions.

	Model A	Model B	Model C	Model D	Experimental
T_1	1216[a]	1000	703	703	703η[b]
T_2	1009	940	725	725	725η[b]
T_3	719	740	531	531	531η[b]
$T_{MG}^{(1)}$	1821				
$T_{MG}^{(2)}$	1017				
$\Delta H(\frac{1}{4},800)$		−1.01[c]	−1.02	−0.98	−1.06
$\Delta H(\frac{1}{2},800)$	−0.39[c]	−1.31[c]	−1.39	−1.38	−1.22
$\Delta H(\frac{3}{4},800)$	−0.06	−0.79	−0.78	−0.90	−0.72
X_1	0.244	0.250	0.254	0.250	0.25
X_2	0.490	0.490	0.492	0.490	0.50
X_3	0.688	0.690	0.696	0.713	0.75

[a]Triple point for equilibrium between two disordered phases and CuAu, see Fig. 4.
[b] $\eta=0.9425$ is the fact converting CVM temperatures into the more accurate Monte Carlo results (see Sec. V).
[c]Although the ordered phases are stabler at these compositions and temperatures, the disordered phases still exist and their enthalpy can be calculated.

Ag-Au (Fig. 6) we predict at low temperatures *stably ordered* compounds since both $\varepsilon^{(n)}$ and $\Delta H^{(n)}$ are negative. Since these ordered phases both for Cu-Ag and for Ag-Au are predicted to occur at low temperatures, they may be difficult to detect.

Figures 7–9 show the calculated mixing enthalpies [Eq. (10)] of these alloys, compared with the experimental values.[1] The predicted order-disorder temperatures, mixing enthalpies at $T=800$ K, and critical compositions for the Cu-Au system are summarized in the first column of Table VII. The fifth column of Table VIII gives the calculated and measured[1] partial molar enthalpies of solution, where they are also compared with the recent calculation of Foiles *et al.*[63]

The results of model A can be summarized as follows.

(i) The general *qualitative* features of the phase diagrams are correctly reproduced. The phase diagrams of Cu-Ag and Ag-Au agree quantitatively with the limited data available (high temperatures only). The new results at lower temperatures (ordered phases for Cu-Ag and Ag-Au) are offered as predictions.

(ii) The *quantitative* description of the Cu-Au phase diagram is poor: Critical order-disorder temperatures (for Cu_3Au this is a peritectic point, whereas for CuAuI and $CuAu_3$, Fig. 4 shows a congruent point) are too high by 200–500 K (Table VII) even after the usual overestimation of critical temperatures by CVM relative to the more accurate Monte Carlo is taken into account (by the constant η in Table VII). Furthermore, two miscibility gaps (dashed areas in Fig. 4) appear in the calculation, with no counterpart in the experimental data.

(iii) The mixing enthalpies of Ag-Au (Fig. 9) as well as

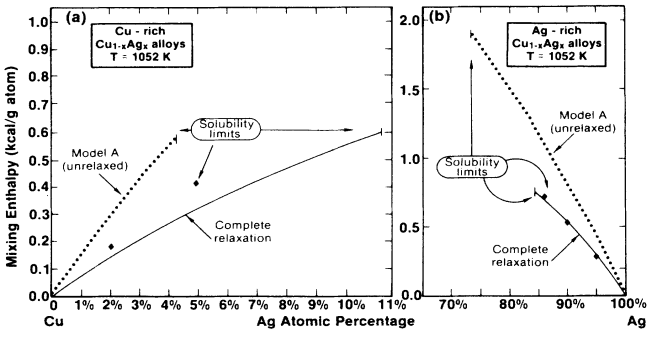

FIG. 8. Calculated excess mixing enthalpies for Cu-Ag at 1052 K in the (a) Cu-rich, and (b) Ag-rich limits. Results are given both for the unrelaxed structures (model A, giving mixing enthalpies that are too positive) and for the fully relaxed structures [model D, with $K=1$ in Eqs. (24) and (25)]. The diamond-shaped symbols give the experimental results (Ref. 1).

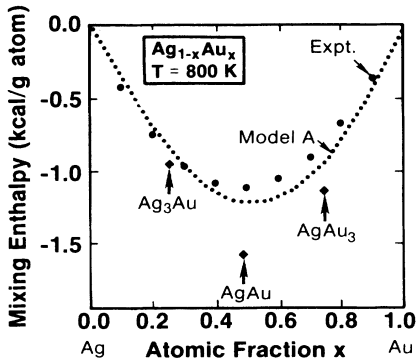

FIG. 9. Calculated excess mixing enthalpies of Ag-Au at 800 K, using the unrelaxed energies of model A, compared with the experimental data (Ref. 1, denoted as solid circles). The formation enthalpies of the *ordered* phases are denoted by the diamond-shaped symbols.

TABLE VIII. Calculated and measured partial molar enthalpies of solution in kcal/g-at.

Alloy	Partial molar enthalpies	Ω_{exptl}[a]	Relaxed energies (model D)	Unrelaxed energies (model A)	Embedded atom[b]
$Cu_{1-x}Au_x$	Au in Cu (Ω_0)	−3.9 (800 K)	−2.4[c]	+6.0	−4.1
	Cu in Au (Ω_1)	−2.8 (800 K)	−3.2[c]	+3.5	−2.8
$Ag_{1-x}Au_x$	Au in Ag (Ω_0)	−4.8 (800 K)		−3.9	−2.5
	Ag in Au (Ω_1)	−4.0 (800 K)		−4.6	−2.5
$Cu_{1-x}Ag_x$	Ag in Cu (Ω_0)	+9.2[d] (1052 K)	+7.1[e]	+15.4	+2.5
	Cu in Ag (Ω_1)	+6.0[d] (1052 K)	+6.3[e]	+9.5	+4.1

[a]Reference 1.
[b]Reference 63.
[c]Relaxation parameter $K=0.2077$.
[d]Data of Ref. 1, available at $x=0.05$ and $x=0.98$.
[e]Full relaxation $K=1$ [Fig. 5(b)].

its partial molar enthalpies of solution (Table VIII) are correctly reproduced. The corresponding results for Cu-Ag (Fig. 8 and Table VII) are too large relative to experiment, whereas for Cu-Au (Fig. 7 and Table VIII) the enthalpies are yet larger, becoming even *positive,* in contrast with experiment.[1]

These discrepancies are consistent with the local density *overestimation* of the strain energy (e.g., lattice mismatch in Table III) and its *underestimation* of the formation enthalpies (e.g., $\Delta H^{(n)}$ in Table III). Since the Ag-Au system is naturally lattice matched, our model correctly predicts the properties of this system. The problem is more acute for the Cu-Au system which has both larger local-density errors and larger elastic energies.

IV. MODEL B: USING THE LOW-TEMPERATURE EXPERIMENTAL DATA FOR ORDERED COMPOUNDS

Having identified an obvious source of error in model A—the insufficiently accurate description of the equilibrium properties of ordered intermetallic phases by the local density approach—we proceed in model B and correct the values of $\{a_{eq}^{(n)}, B^{(n)}, \text{ and } \Delta H^{(n)}\}$ for Cu_nAu_{4-n} to match the experimentally observed values of these ordered structures at low temperatures (second column in Table VI, labeled model B). Our objective here is to find whether the use of nearly-perfect data on the five basic ordered compounds at low temperatures would suffice to describe the phase diagram in a full temperature and composition range. The resulting phase diagram of Cu-Au is shown in Fig. 10; the mixing enthalpy is shown in Fig. 7(b). Table VII gives the critical temperatures and enthalpies.

The results of model B can be summarized as follows.

(i) The unphysical miscibility gaps of model A (Fig. 4) have disappeared (Fig. 10).

(ii) The mixing enthalpies are very close to experiment (Fig. 7); Table VII shows in fact that they are within 0.09 kcal/g-at. of experiment.

(iii) The critical order-disorder temperatures (Table VII) are too high relative to experiment (after correcting for the overestimation of CVM relative to Monte Carlo) by 300 K ($Cu_3Au \rightleftarrows Cu_{0.75}Au_{0.25}$), 215 K (for $CuAu \rightleftarrows Cu_{0.5}Au_{0.5}$) and by 210 K (for $CuAu_3 \rightleftarrows Cu_{0.25}Au_{0.75}$).

We conclude that the use of five basic unrelaxed ordered structures with "exact" structural and thermodynamic parameters as building blocks is sufficient to reproduce the excess thermodynamic functions of the disordered phase and the qualitative features of the phase diagram, but overestimates critical order-disorder temperatures by ~200–300 K. While the ability to describe the temperature-composition properties of an *alloy* from the properties of *five ordered structures* at low temperatures constitutes a significant accomplishment, we wish to identify the physical factors which would

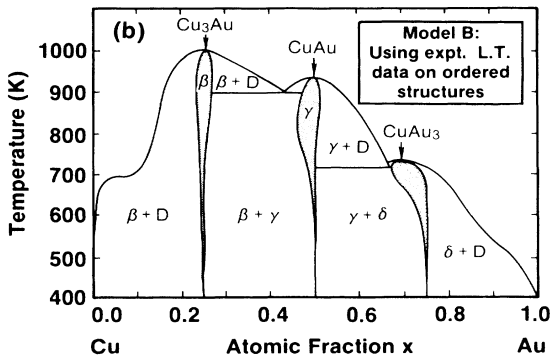

FIG. 10. Calculated phase diagram of Cu-Au using the *observed* equilibrium properties of the five ordered phases at low temperature (L.T.) (Table VI). Shaded areas denote ordered structures. Observe that the unphysical miscibility gaps present in model A (Fig. 4) have disappeared, and that the order-disorder transition temperatures are lower.

lead to an even closer agreement with experiment.

V. MODEL C: SENSITIVITY OF THE PHASE DIAGRAM TO THE STRUCTURAL PARAMETERS OF THE ORDERED PHASES

Our foregoing discussion shows that the use of the properties of five *physically realizable* ordered intermetallic phases to construct the phase diagram leads to an overestimation of the critical temperatures. Given the fact that the extremely small differences in the structural properties of the ordered phases in model A relative to model B (see Table VI) resulted in substantial changes in the critical temperatures (Table VII), one wonders if similarly small changes in the parameters used *in model B* could produce an accurate phase diagram. We want then to establish the *magnitude* of the changes in $\{a_{\rm eq}^{(n)},\Delta H^{(n)}\}$ needed to reproduce the observed phase diagram. In other words, having established in model B that the *real* ordered structures A_nB_{4-n} alone are insufficient to accurately reproduce critical order-disorder temperatures, we now ask what are the values of $\{a_{\rm eq}^{(n)},\Delta H^{(n)}\}$ of "*effective ordered structures*" A_nB_{4-n} needed to get an "exact" phase diagram.

Since fitting only three critical temperatures by adjusting the numerous values of $\{a_{\rm eq}^{(n)},B^{(n)},\Delta H^{(n)}\}$ may be an overdetermined problem (if not an uninformative exercise), we set a number of simple restrictions on the problem. (i) We will not adjust $\{B^{(n)},B_p^{(n)}\}$ but keep them fixed as in model B. (ii) We require obtaining not only the three critical temperatures but also a physically correct phase diagram (e.g., no miscibility gap as in model A). (iii) All $a_{\rm eq}^{(n)}$ should be shifted by adjusting a *single parameter* Ω in a function $a^{(n)}(\Omega)$. This is done by observing[26] that $Z(x)$ of Eq. (20) can be approximated as a constant 2Ω. Integrating $V(x)$ from Eq. (20) then yields

$$V(x)=\left[[V(0)]^{1/2}+(\tfrac{1}{2}\Omega)^{1/2}\int_0^x\frac{dX}{[B(X)]^{1/2}}\right]^2, \qquad (23)$$

which we use to define a scaling relationship for the equilibrium molar volumes $V_n=V(X_n)$ at the stoichiometric compositions $x=X_n$, as functions of Ω. Interpolating the $B^{(n)}$ values to obtain $B(x)$ and using Eq. (23) we end up with five molar volumes *functions* of a single parameter Ω. By varying Ω we can fit $T_1=703$ K, $T_2=725$ K, $T_3=531$ K if we simultaneously perform small shifts in the values of $\Delta H^{(1)}$ and $\Delta H^{(3)}$ [we keep $\Delta H^{(2)}$ fixed since it is the most reliably determined formation enthalpy in this system. Shifting $\Delta H^{(3)}$ is no violation of any experimental data because it was interpolated, not measured (Table III). On the other hand, $\Delta H^{(1)}$, though well measured is the enthalpy of formation on ill-defined phase: A compound presenting different lattice parameters and possibly enthalpies, corresponding to different states of order]. The parameters for fitting then became $\Delta H^{(1)}$, $\Delta H^{(3)}$, and Ω. (The dependence of the transition temperatures on $\Delta H^{(1)}$ and $\Delta H^{(3)}$ is considerably weaker than the dependence on the lattice parameters.) The resulting lattice parameters and enthalpies for model C are given in Table VI. The resulting phase diagram is shown in Fig. 11 and is nearly identical to the experimental phase diagram, where it is known (of course one must account for the factor $\eta=0.9425$ that corrects the CVM calculation).

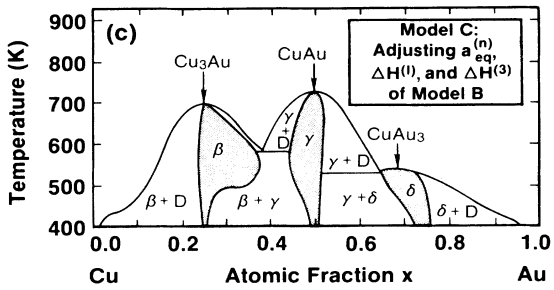

FIG. 11. Calculated phase diagram of Cu-Au using slight adjustments of $a_{\rm eq}^{(n)}$, $\Delta H^{(1)}$, and $\Delta H^{(3)}$ of model B (Table VI). These small changes result in significant modifications in the phase diagram relative to the unmodified model B (Fig. 10), making this phase diagram very close to experiment [Fig. 1(a)].

This exercise shows that *a change in the equilibrium lattice parameters of the experimentally observed ordered structures (model B) by only* ~ 0.04 Å *(*$\sim 1\%$*), and a change of* ~ 0.1 *Kcal/g-at. in the formation enthalpies is sufficient to produce a perfect fit to the phase diagram (to within* ~ 1 *K) and mixing enthalpies, using but five ordered structures.* This emphasizes the critical need to establish lattice parameters with extreme precision if the system consists of two components with a large lattice mismatch. Clearly, the structures corresponding to the $\{a_{\rm eq}^{(n)},\Delta H^{(n)}\}$ values of model C are fictitious: They represent the "effective medium" properties of the five hypothetical basic structures which produce, by construction, a perfect phase diagram. However, the fact that the properties of these fictitious structures are so close to those of the real structures, combined with our foregoing discussion on the role of lattice relaxation (Sec. II C), suggest to us a *physical* way of producing a correct phase diagram, which we discuss next.

VI. MODEL D: EFFECTS OF LATTICE RELAXATIONS

A. The relaxation model

In using models A and B we have assumed that (i) the equilibrium volumes $V_{\rm eq}^{(n)}(x)$ of the tetrahedra A_nB_{4-n} *embedded in an alloy* of composition x equal the values $V_{\rm eq}^{(n)}(X_n)\equiv V^{(n)}$ for the *pure* tetrahedra A_nB_{4-n}, and (ii) no *local* distortions occur around a given tetrahedron. Our foregoing discussion (Sec. II C) indicated that the coexistence of numerous types of tetrahedra could affect the properties of any given tetrahedron, including its equilibrium volume and its local structure. To generalize our first assumption (i) above we note that to first order in a Taylor series, the equilibrium volume of structure n at a composition x is

$$V_{\rm eq}^{(n)}(x)=V_{\rm eq}^{(n)}(X_n)+K_n[V(x)-V_{\rm eq}^{(n)}(X_n)]+\cdots, \qquad (24)$$

where K_n are constants, and where $V(x)$ is the *equilibri-*

um volume of the alloy at the composition x. Since for small volume changes the energy scales as $[V(x)-V_{\rm eq}^{(n)}(x)]^2$, Eq. (24) shows that the energy of a cluster embedded in an alloy of molar volume $V(x)$ is

$$\Delta E[n,V(x)]=\Delta H^{(n)}+\frac{1}{2}\frac{B^{(n)}}{V^{(n)}}(1-K_n)^2 \times[V(x)-V^{(n)}]^2+\cdots , \quad (25)$$

where $\Delta H^{(n)}$ is the value at $V=V^{(n)}$ and $V^{(n)}\equiv V_{\rm eq}^{(n)}(X_n)$. Here $V(x)$ is found by solving[64]

$$\left.\frac{d\Delta E[\sigma,V]}{dV}\right|_x=\sum_n P_n(x,T)\frac{B^{(n)}}{V^{(n)}}(1-K_n) \times[V(x)-V^{(n)}]=0 . \quad (26)$$

The graphical interpretation of Eq. (24) is given in Fig. 12. Had one used the equilibrium volumes $V_{\rm eq}^{(n)}(X_n)\equiv V^{(n)}$ of the ordered A_nB_{4-n} structures for *all* compositions x (i.e., set $K_n\equiv 0$), the five solid lines in Fig. 12 would have been horizontal. This corresponds to models A and B where we assumed that each tetrahedron of type n can be characterized by a volume $V^{(n)}$ which is independent of its chemical environment.

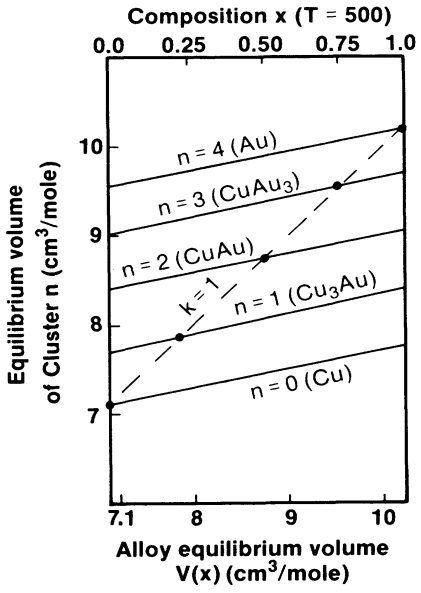

FIG. 12. Schematic plot of the composition dependence of the equilibrium molar volumes $V_{\rm eq}^{(n)}(x)$ of ordered tetrahedra n in a medium of composition x [see Eq. (24)]. Solid circles denote the values of $V_{\rm eq}^{(n)}(X_n)$ for the perfectly ordered phases A_nB_{4-n} at stoichiometric compositions $X_n=0,\frac{1}{4},\frac{1}{2},\frac{3}{4}$, and 1. The unrelaxed model ($K=0$) corresponds to the case where all solid lines are horizontal and each passes through the corresponding $V_{\rm eq}^{(n)}(X_n)$ value. The fully relaxed model ($K=1$) corresponds to the case where all five lines collapse into the single dashed line passing through all $V_{\rm eq}^{(n)}(X_n)$ values.

While this assumption (analogous to the classical concept[62,65] of the existence of transferable atomic radii) has been the cornerstone of structural chemistry since Bragg[65] and Pauling[62] demonstrated that numerous packing arrangements of the same atoms in different compounds can be explained by assuming fixed atomic volumes (or radii), it is probably insufficiently accurate for *phase-diagram* calculations, given their extreme sensitivity to small changes of $V^{(n)}$ (Sec. V). The effect of $K_n\neq 0$ is then to allow for such internal relaxations. Notice that $K_n\neq 0$ does not imply any changes in bond distances of tetrahedron A_nB_{4-n} in the alloy, but merely that the *equilibrium* values of $V_{\rm eq}^{(n)}(x)$ equal those of the pure ordered compounds $V_{\rm eq}^{(n)}(X_n)$ only at $x=X_n$. The opposite extreme to $K_n=0$ is $K_n=1$ (dashed line in Fig. 12), where all of the *distinct* volumes $V_{\rm eq}^{(n)}(x)$ become n independent [equaling $V(x)$], as in the virtual lattice model. This viewpoint argues that atoms lose their identities in an alloy, forming effectively "average atoms" with correspondingly average atomic volumes.

Rather than seek a *set* of n-dependent K_n values, we instead pose the following question: Does there exist a *single* effective relaxation parameter K for a given binary alloy which when applied to the properties of the five actual ordered phases (model B) cures all of the discrepancies of this phase diagram and thermodynamic properties relative to experiment? This reduction to a single n-independent relaxation parameter also simplifies the problem since $V(x)$ and $B(x)$[64] becomes K dependent only indirectly through $P_n(x,T)$ [as $(1-K)$ can be taken out of the sum over n in Eq. (26)].

In addition to cell-internal relaxation modeled by $K\neq 0$, one could envision local atomic cell-external relaxations to take place [i.e., avoid our second assumption (ii)]. These[53] are equivalent to the use of a large number of basic ordered structures which taken together are able to describe arbitrary local displacements of a given site. Such *local* relaxations could be described by using *large* supercells (instead of the 4-atom cell of the structures used here, see Fig. 2). They could lower the strain energy and raise the configurational entropy (providing more configurational degrees of freedom). Both effects then tend to reduce the free energy of the disordered phase, lowering thereby order-disorder transition temperatures. Rather than model separately the cell-internal and cell-external relaxation effects (which are clearly beyond the nearest-neighbor tetrahedron approximation), we instead seek effective (global) relaxation parameters K in the sense of Eqs. (24)–(26).

B. Results for the relaxation model

1. Cu-Au

Keeping $\{a_{\rm eq}^{(n)},B^{(n)},B_p^{(n)},\Delta H^{(2)}\}$ fixed at the values of model B (see Table VI) we then adjust $\{K,\Delta H^{(1)},\Delta H^{(3)}\}$. Solving the Cu-Au CVM phase diagram with these adjustable values produces the parameters shown in Table VI as "model D." The phase diagram is given in Fig. 13, the mixing enthalpy in Fig. 7, and the critical data is summarized in Table VII. The limiting partial enthal-

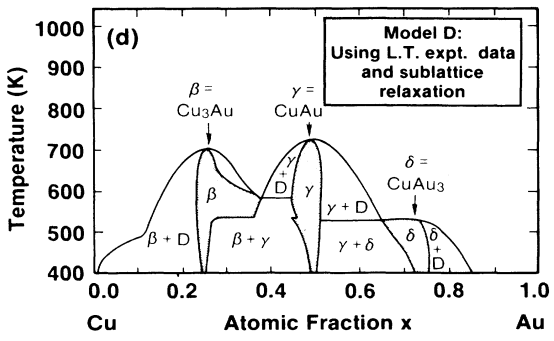

FIG. 13. Calculated phase diagram of Cu-Au using a single relaxation parameter $K=0.2077$ (Table VI) and the results of model B. Observe the nearly perfect fit with the experimental phase diagram of Fig. 1(a).

pies resulting from model D are shown in Table VIII. A perfect fit is obtained for $K=0.20772$, indicating that Pauling's view ($K=0$) is only $\sim 20\%$ wrong, whereas the virtual lattice result ($K=1$) is $\sim 80\%$ wrong. A perfect fit is also possible starting from the first-principles results of model A, producing a somewhat different value of the relaxation parameter K. Hence, *quantitatively precise phase diagrams and thermodynamic properties of alloys can be obtained using a small number of modestly relaxed ordered building blocks.* This is the basic finding of this work.

In solving the phase diagram problem we minimize the grand canonical potential $\tilde{G}(x,T)$ both with respect to $\xi_n(\sigma)$ [Eq. (5)] and with respect to the alloy volume $V(x)$. [Notice that in CVM the probabilities $P_n(x,T)$ are variational, i.e., $\partial\tilde{G}/\partial P_n=0$. The minimization with respect to the volume, i.e., $d\tilde{G}/dV=0$ is reduced to an equation for the partial derivative $\partial\tilde{G}/\partial V=0$.] The results of this procedure for the volume $V(x,T)$ are depicted in Table IX for $T=500$ K, 800 K, and for the random disorder approximation ($T=\infty$). They are compared with the volume $V_{\rm eq}^{(n)}(X_n)$ of the perfectly ordered compounds. We find that there is a volume discontinuity upon order-disorder transformation for all three cases, i.e., $Cu_3Au \rightleftarrows Cu_{0.75}Au_{0.25}$; $CuAu \rightleftarrows Cu_{0.5}Au_{0.5}$, and $CuAu_3 \rightleftarrows Cu_{0.25}Au_{0.75}$. The discontinuity is larger for Cu_3Au and smaller for $CuAu_3$. [While we find the transition region to be very narrow (less than 0.1 K) for Cu_3Au, for $CuAu_3$ the region extends in a range of almost 40 K. The discontinuities for CuAu and $CuAu_3$ are very difficult to observe experimentally because, in the case of CuAu there is a tetragonal distortion when crossing the region, while, for $CuAu_3$, the transition region is so broad and the volume discontinuity so small that it is unlikely that the internal strains could prevent the formation of multiphase domains. On the other hand, the discontinuity of Cu_3Au has been observed to be some thousandths of Å,[66] while our calculated result is 0.0080 Å, in reasonable agreement with experiment.]

2. *Cu-Ag*

Since only Cu-Au and Cu-Ag show a significant lattice mismatch between the constituents we include relaxation only for these systems (the results of the unrelaxed model A for Ag-Au are already adequate). Since the data on Cu-Ag is limited, one cannot narrowly determine the relaxation parameter, as was done for Cu-Au. We therefore examine the extreme limits of $K=0$ (no relaxation, model A) and $K=1$ (full relaxation). Table VIII shows that the partial solution enthalpies in the fully relaxed calculation (7.1 and 6.3 kcal/g-at. for Ag-in-Cu and for Cu-in-Ag, respectively) are closer to the observed values (9.2 and 6.0, respectively) than are the unrelaxed values (15.4 and 9.5, respectively). Figure 8 shows that the observed mixing enthalpies for small dilution are indeed closer to those obtained from the relaxed model. Figure 5(b) shows the phase diagram with full relaxation and demonstrates a considerable reduction in the miscibility temperature (which remains, however, above the melting line).

VII. AVERAGE PROPERTIES OF THE ALLOYS

Having established an accurate model (D) for the phase diagrams of noble metals, involving a single adjustable (relaxation) parameter, we proceed to investigate some of the properties of these calculated phase diagrams.

TABLE IX. Comparison of the equilibrium molar volumes $V_{\rm eq}^{(n)}$ of the ordered phase Cu_nAu_{4-n} (from $a_{\rm eq}^{(n)}$ of Table III) with those of the alloy $V(X_n,T)$ at compositions $X_n=0$, $\frac{1}{4}$, $\frac{1}{2}$, $\frac{3}{4}$, and 1, as calculated from model D. Percentage changes of the alloy volume relative to the ordered compounds are given in parentheses. Thermal expansion effects are excluded. Note the large change in molar volume associated with disordering Cu_3Au.

Ordered structure	Alloy composition $Cu_{1-x}Au_x$	$V_{\rm eq}^{(n)}$ ordered phase	V ($T=500$)	V ($T=800$)	V ($T=\infty$)
Cu	0.0	7.111	7.111 (0.00%)	7.111 (0.00%)	7.111 (0.00%)
Cu_3Au	0.25	7.892	7.962 (0.89%)	7.982 (1.14%)	8.050 (2.0%)
CuAu	0.50	8.698	8.752 (0.62%)	8.769 (0.82%)	8.836 (1.58%)
$CuAu_3$	0.75	9.506	9.543 (0.39%)	9.550 (0.46%)	9.571 (0.68%)
Au	1.0	10.213	10.213 (0.00%)	10.213 (0.00%)	10.213 (0.00%)

Figure 14 depicts the excess probabilities

$$\Delta P_n(x,T)=P_n(x,T)-P_n^{(R)}(x) \tag{27}$$

with respect to the random (R) probabilities, as a function of temperatures, demonstrating that even for very high temperatures (~ 2000 K) the clusters Cu_3Au, CuAu, and $CuAu_3$ exist considerably *in excess* ($>10\%$) of what random statistics would predict. Simple random disorder models are hence inapplicable. Figure 15 shows $\Delta P_n(x,T)$ as a function of composition, demonstrating that the *mixed tetrahedra* (Cu_nAu_{4-n} for $n=1$, 2, and 3) exist in excess, whereas the *pure* tetrahedra ($n=0$ and 4) are deficient. This "clustering" phenomena leads to pronounced nonideal behavior of the enthalpy and entropy. Defining the "interaction parameters"

$$\begin{aligned}\Omega_S(x,T)&=\Delta S(x,T)/x(1-x)\ ,\\ \Omega_H(x,T)&=\Delta H(x,T)/x(1-x)\ ,\\ \Omega_F(x,T)&=\Delta F(x,T)/x(1-x)\ ,\end{aligned} \tag{28}$$

where $\Delta S(x,T)$ is the *nonideal* mixing entropy, $\Delta H(x,T)$ [Eq. (10)] is the mixing enthalpy, and $\Delta F(x,T)$ is the excess free energy of mixing, Fig. 16 shows for Cu-Au large *negative values* of Ω_S, Ω_H, and Ω_F; only for "$T=\infty$" do $\Omega_H(x,T)=\Omega_F(x,T)$ become nearly composition independent. It is interesting to note that the unrelaxed results (model A) give a *positive* $\Omega_H(x,T)$ [Fig. 7(a)] if random probabilities are used, whereas the use of the variational probabilities gives correctly a negative $\Omega_H(x,T)$, both for model A [Fig. 7(b)] and for model D (Fig. 16). In contrast to the strong composition-dependent interaction parameters for Cu-Au, the Ag-Au system (Fig. 17) exhibits only a weak composition dependence in $\Omega(x,T)$. These trends were indeed observed experimentally:[67] For Ag-Au $\Omega_H(x,T)$ is nearly x independent, whereas for Cu-Au it is strongly composition dependent.

Figures 16 and 17 show *negative* values for the excess mixing entropies $\Omega_S(x,T)$ for Cu-Au and Ag-Au. Whereas Hultgren *et al.*[1] quote indeed negative values for Ag-Au, in agreement with our results, they give positive (but extremely small) values for Cu-Au at 800 T. More recent experimental studies of Kleppa and Topor[67] give, however, negative values, as we find in Fig. 16.

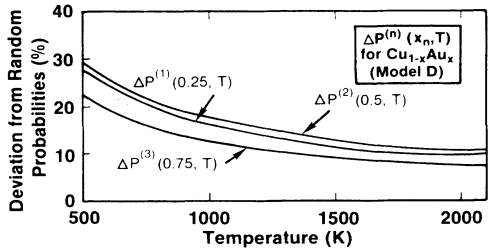

FIG. 14. The difference $\Delta P^{(n)}(x,T)$ of the actual cluster probabilities $P^{(n)}(x,T)$ and the random probabilities $P_R^{(n)}(x)$ for Cu-Au, calculated from model D. Observe that the actual probabilities deviate significantly from random probabilities even for very high temperatures.

One can compare the mixing enthalpies $\Delta H(x_n,T)$ of the disordered alloy at stoichiometric compositions X_n (Table VII) with the formation enthalpy $\Delta H^{(n)}$ of the ordered phases at the same compositions (Table VI) to deduce the "ordering energies" $\lambda^{(n)}(T)=\Delta H^{(n)}-\Delta H(X_n,T)$. This yields for Cu_nAu_{4-n} at $T=800$ K

$$\begin{aligned}\lambda^{(1)}&=-1.56+0.98=-0.58\ \text{kcal/g-at.}\ ,\\ \lambda^{(2)}&=-2.1+1.38=-0.72\ \text{kcal/g-at.}\ ,\\ \lambda^{(3)}&=-1.37+0.90=-0.47\ \text{kcal/g-at.}\ ,\end{aligned} \tag{29}$$

showing that CuAu($n=2$) has the strongest tendency to order. Had one used instead the much higher mixing enthalpies $\Delta H(x,T)$ of the *random* alloy [Fig. 16(d)], the ordering energies $\lambda^{(n)}$ would have been considerably more negative. In the extreme limit of the unrelaxed model A [Fig. 7(a)], $\Delta H^{(n)}$ has the opposite sign to $\Delta H(X_n, T=\infty)$. This unphysical result is apparent in the work of Terakura *et al.*[2] who have combined unrelaxed energies with random statistics.

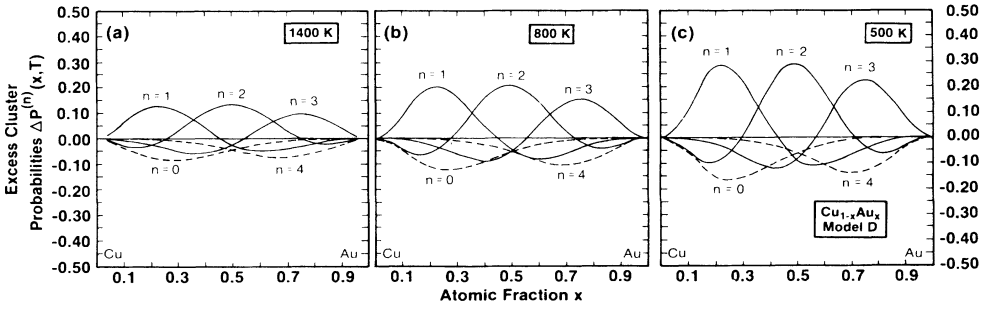

FIG. 15. Excess cluster probabilities $\Delta P^{(n)}(x,T)$ (relative to random probabilities) for Cu-Au in model D. Note that the clusters Cu_3Au, CuAu, and $CuAu_3$ exist in *excess* of what random statistics would grant around at $x=\frac{1}{4}$, $\frac{1}{2}$, and $\frac{3}{4}$, respectively, whereas the cluster Cu_4 and Au_4 are *deficient* at all compositions.

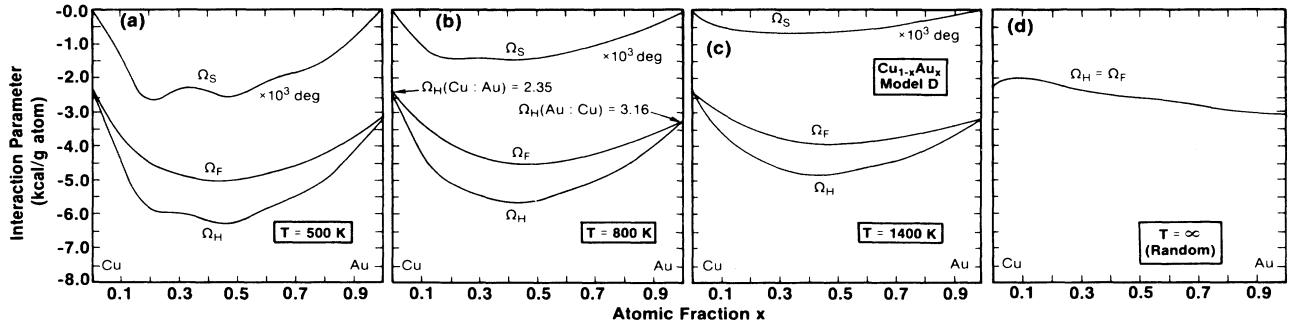

FIG. 16. Interaction parameters [Eq. (28)] for the enthalpy (Ω_H), entropy (Ω_S), and free energy (Ω_F) of Cu-Au in model D. Observe that Ω_S is negative and that the Ω_S, Ω_H, and Ω_F are significantly composition dependent, in agreement with experiment [Ref. (67)], unless one assumes random probabilities (d). The arrows in (b) point to the limiting partial mixing enthalpies $\Omega_H(0)$ and $\Omega_H(1)$ (Table VIII).

VIII. SUMMARY

We have analyzed the extent to which the phase diagrams and excess thermodynamic functions of noble-metal alloys can be described through the nearest-neighbor fcc Ising model with volume-dependent interaction energies determined from the properties of five ordered A_nB_{4-n} ($0 \le n \le 4$) phases. We find the following conclusions.

(i) Using the energies of the five ordered phases obtained from first-principles total energy calculations on unrelaxed structures (model A) one can obtain qualitatively correct phase diagrams and mixing enthalpies, and analyze their trends in terms of the electronic structure of the constituents. The order-disorder transition temperatures are, however, too high by $\sim$200–500 K, and spurious miscibility gaps appear for Cu-Au.

(ii) In attempting to analyze what fraction of the errors result from the imperfect description by the local density formulation of the ground-state properties of the five ordered phases, we have used the low-temperature experimentally observed properties of these structures (model B). We find substantial improvements, including the disappearance of the spurious miscibility gaps for Cu-Au and a near-perfect reproduction of mixing enthalpies. Order-disorder critical temperatures are, however, still too high by 200–300 K.

(iii) Studying the sensitivity of the phase diagrams to small changes in the structural parameters of the ordered phases, we find that a mere change of 0.04 Å (1%) of lattice parameters and $\sim$0.1 Kcal/g-at. in formation enthalpies of the ordered phases suffices to bring model B into perfect agreement with experiment. Given this sensitivity, we introduce lattice relaxation effects.

(iv) Our total-energy calculations on phases exhibiting two different types of tetrahedra (A_3B and AB_3) in the same cell show "relaxation effects," (i.e., a modification in the elastic energy of a given tetrahedron due to the presence of other types of tetrahedra). We model both such "cell-internal" as well as "cell-external" relaxation effects (e.g., *local* relaxations) by allowing the *equilibrium* volume of each tetrahedron to depend on the average alloy composition: Using but a single relaxation parameter K (zero when no relaxation occurs, one when it is complete) and the structural parameters of model B (or model A) we find a perfect fit to the phase diagram for $K \cong 0.2$. Such rather modest relaxation effects hence account for the full details of the phase diagram even when only five basic ordered "building blocks" are used. We investigate the properties of model D by studying in detail the excess thermodynamic functions and the clustering phenomena. Finally, we compare the results of

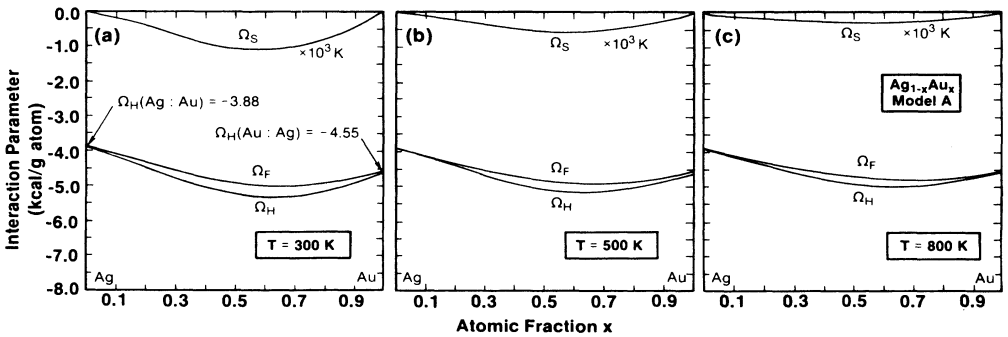

FIG. 17. Interaction parameters [Eq. (28)] for the enthalpy (Ω_H), entropy (Ω_S), and free energy (Ω_F) of Ag-Au in model A. Observe that in contrast with Cu-Au (Fig. 16), these depend only weakly on temperature and composition. The arrows in (a) point to the limiting partial mixing enthalpies $\Omega_H(0)$ and $\Omega_H(1)$ (Table VIII).

model D to those obtained by the simpler ε-G approach[26] (see the Appendix).

ACKNOWLEDGMENT

This work was supported in part by the Office of Energy Research, Materials Science Division, U.S. Department of Energy, under Grant No. DE-AC02-77-CH00178.

APPENDIX: COMPARISON OF THE ε-G APPROACH AND THE PRESENT EQUATION-OF-STATE APPROACH TO THE PHASE DIAGRAM PROBLEM

Our present approach to the phase diagram of a binary A_xB_{1-x} system is based on representing the excess energy $\Delta E(\sigma,V)$ of the alloy in a state of order σ as a superposition of equations of states $\Delta E(n,V)$ of the ordered structures A_nB_{4-n}

$$\Delta E(\sigma,V)=\sum_n \Delta E(n,V)\xi_n(\sigma)\ , \tag{A1}$$

and determining the correlation functions $\xi_n(\sigma)=\xi_n(x,T)$ by solving this Ising Hamiltonian using $\{\Delta E(n,V)\}$ as input. These $\Delta E(n,V)$'s are the excess energies of an ordered structure A_nB_{4-n} with respect to the energies of equivalent amounts of A and B at their respective equilibrium volumes V_A and V_B

$$\Delta E(n,V)=\tfrac{1}{4}E[A_nB_{4-n};V]-\frac{n}{4}E_A(V_A)-\frac{4-n}{4}E_B(V_B)\ . \tag{A2}$$

Ferreira *et al.*[26] have proposed an alternative approach which is simpler, but requires that the molar volumes of the thermodynamically selected configurations be approximately state of order independent. In this "ε-G model" $\Delta E(n,V)$ is replaced by a *separable* form

$$\Delta\tilde{E}(n,V)=\varepsilon^{(n)}+\left[(1-X_n)\int_0^{X(V)}xZ(x)dx+X_n\int_{X(V)}^1(1-x)Z(x)dx\right]\ , \tag{A3}$$

where $\varepsilon^{(n)}$ are the "chemical energies," and $Z(x)$ is given by

$$Z(x)=\frac{B(x)}{V(x)}\left[\frac{dV}{dx}\right]^2\ . \tag{A4}$$

Here the constant $\varepsilon^{(n)}$ is the volume-independent "chemical energy," $V(x)$ and $B(x)$ are the equilibrium volume and bulk modulus of the alloy, both functions of the concentration x, but otherwise independent of the state of order, $X(V)$ is the inverse function of $V(x)$, and X_n is the stoichiometric concentration in the ordered compound n. At the equilibrium volume of the alloy, the enthalpy is

$$\Delta H(x,T)=\sum_n P_n(x,T)\Delta\tilde{E}(n,V_{\rm eq})=\sum_n P_n(x,T)\varepsilon^{(n)}+G(x)\ , \tag{A5}$$

where $P_n(x,T)$ are the thermal average of the correlation function $\xi_n(x,T)$ and

$$G(x)=(1-x)\int_0^x x'Z(x')dx'+x\int_x^1(1-x')Z(x')dx' \tag{A6}$$

because $X(V_{\rm eq})=x$. From Eqs. (A3) and (A6) one has

$$\Delta\tilde{E}(n,V_{\rm eq})=\varepsilon^{(n)}+G(X_n)\equiv\Delta H^{(n)}\ . \tag{A7}$$

In this Appendix we compare these two approaches. Comparing $\Delta E(n,V)$ of Eq. (A2) to $\Delta\tilde{E}(n,V)$ of Eq. (A3) we note the following.

(i) Both have the same value at equilibrium (a value which equals the formation enthalpy $\Delta H^{(n)}$ of the ordered phase n) since $\varepsilon^{(n)}$ is calculated from the same given $\Delta H^{(n)}$ value [Eq. (A7)].

(ii) The minimum occurs at the same equilibrium volume $V_{\rm eq}^{(n)}=V(X_n)$, since the given $\{V_{\rm eq}^{(n)}\}$ are used to construct $Z(x)$ of Eq. (A4).

(iii) The second volume derivatives of these excess energies [bulk modulus $B^{(n)}=B(X_n)$] are the same since $\{B^{(n)}\}$ is used to construct $Z(x)$ of Eq. (A4).

(iv) The third volume derivatives of the excess energies are, in general, not the same. In the ε-G approach these are related to higher-order composition derivatives of $V(x)$ and $B(x)$, whereas in the present equation of state approach the third volume derivative of the energy gives the pressure coefficient $B_p^{(n)}$ of the bulk modulus.

To assess the role of $B_p^{(n)}$ on the phase diagram we have recalculated the phase diagram of Cu-Au in model C (Table VI) using our standard equation of state approach, but set all $B_p^{(n)}=-1$. In this case the equation of states of Eq. (A2) reduce simply to the harmonic form

$$\Delta E(n,V)\cong\Delta H^{(n)}+\frac{B^{(n)}}{2V^{(n)}}(V-V^{(n)})^2\ . \tag{A8}$$

Despite the fact that this equation of state is very different away from equilibrium from the Murnaghan equation of state[33] used in this paper, the resulting phase diagrams (Fig. 18) are very similar (compare with Fig. 11). This result implies that at the temperatures considered in these phase diagrams, the Boltzmann population of clusters whose volume departs considerably from $V^{(n)}$ (these are the only clusters which experience

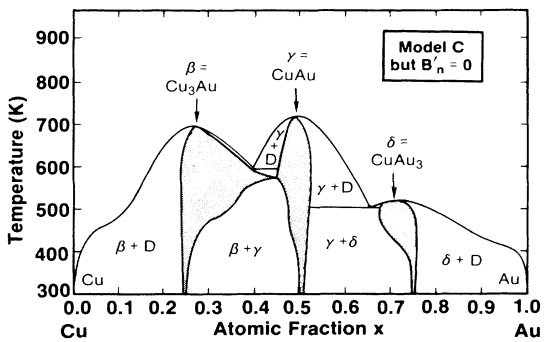

FIG. 18. Calculated phase diagram of Cu-Au using the parameters of model C (Table VI) but setting all $B_p^{(n)}$ to zero. The similarity to the phase diagram of model C (Fig. 11) indicates the relative insignificance of the curvature variation of $\Delta E(n,V)$ for V far from equilibrium.

$B_p^{(n)} \neq 0$) is small. The clustering phenomena observed here (Fig. 15 and Sec. VII) simply suggests that the system reduces the population of the most strained clusters. This weak dependence of the phase diagram on $B_p^{(n)}$ explains the success of the ε-G model. This also implies that the equilibrium alloy volume [which minimizes Eq. (A5)] is reasonably state-of-the-order independent. (The small variations of the volume with changes in the state of order shown in Table IX are, however, missed by the ε-G approach.)

The success of the ε-G approach in practical applications depends on one's ability to simply calculate $Z(x)$. In the equation of state approach this requires solving the phase diagram first. This gives $V(x,T)$ (e.g., Table IX), $B(x,T)$ and $dV(x,T)/dx$ which can be inserted in the definition (A4) of $Z(x,T)$ obtaining a temperature-dependent function. In the ε-G approach one needs to calculate $Z(x)$ *a priori* [to obtain $\varepsilon^{(n)}$ and $G(x)$]; by construction, it is T independent. This is simply done by interpolating $V(x)$ from $\{V^{(n)}\}$ of the ordered phases as

$$V(x)=\sum_n V^{(n)} \prod_{i \neq n} \frac{x-X_i}{X_n-X_i} , \tag{A9}$$

with an analogous expression for $B(x)$. These functions are then used in Eq. (A4), [together with $dV(x)/dx$ also obtained from Eq. (A9)] to obtain $Z(x)$.

We will compare these functions for Cu-Au from model D, using the ε-G and the equation of state approach. (This comparison will be done only for the disordered phase because the ordered solutions only exist at a very small range of x and V. On the other hand, in these small ranges, the parabolic approximation is correct anyway, which validates the ε-G assumption.)

For the ε-G separation of variables [Eq. (A3)] to be valid one requires that the true $Z(x,T)$ will depend but weakly on temperature; for the ε-G construction of $Z(x)$ to be valid we require that it matches closely the $Z(x,T)$ calculated from the equation-of-state approach. To test these assumptions, Fig. 19 shows $Z(x,T)$ for Cu-Au (model D) calculated from the CVM solution to the equation of state representation for $T=500$ K, 800 K, and random-disorder ("$T=\infty$"). It is compared with $Z(x)$ calculated from Eqs. (A4) and (A8) using the data $\{V^{(n)},B^{(n)}\}$ for the ordered compounds given in Table VI. The range of temperatures from 500 to 800 K is specially important because all the phase transitions

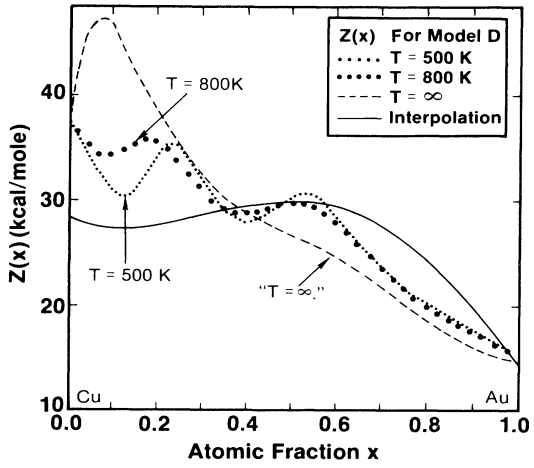

FIG. 19. The calculated function $Z(x,T)$ [Eq. (A4)] for Cu-Au using the present equation of state approach (model D) for $T=500$ and 800 K and $T=\infty$ K, compared with $Z(x)$ calculated in the ε-G approach by interpolating the properties of the five ordered structures [solid line and Eq. (A9)].

occur in this range. One observes that $Z(x,T)$ at $T=500$ K differs very little from that of $T=800$ K, except for the compositions near $x=0.15$ when the difference reaches a maximum of 13%. The curve for $T=\infty$ and that obtained in the ε-G method (solid line) present larger deviations from those of $T=500$ and 800 K.

The four functions $Z(x)$ were used in Eq. (A6) to generate $G(x)$ which was used in Eq. (A7) to calculate the chemical energies $\varepsilon^{(n)}$. The results are presented in Table X which also shows the "effective" $\varepsilon^{(n)}$. These effective chemical energies were obtained in the following way. If the (ε,G) separation were exact, then the critical temperatures would depend only on the $\varepsilon^{(n)}$ and not on $G(x)$. Then, the effective $\varepsilon^{(n)}$ could be calculated by using a simple Ising Hamiltonian fitted to give the critical temperatures of 703, 725, and 531 K, much in the same way as done by De Fontaine and Kikuchi.[15]

From Fig. 19 and Table X one sees how well the (ε,G) separation is working, and how well the interpolation scheme to calculate $Z(x)$ and $\varepsilon^{(n)}$ is satisfactory. Most

TABLE X. Calculation of $\varepsilon^{(n)}$ (in kcal/g-at.) for the Cu-Au system from the parameters of model D. For $T=500$ K, 800 K, and ∞ we use $Z(x,T)$ calculated in CVM (Fig. 19), whereas "interpolation" means that $Z(x)$ was calculated in the ε-G model.

	$T=500$ K	$T=800$ K	$T=\infty$ K	Interpolation	Effective[a]
$\varepsilon^{(1)}$	−4.317	−4.329	−4.388	−4.205	−4.228
$\varepsilon^{(2)}$	−5.618	−5.603	−5.524	−5.630	−5.591
$\varepsilon^{(3)}$	−3.833	−3.813	−3.717	−3.935	−3.860

[a]These are defined as those parameters of the pure Ising model ("ε only") that give the correct T_1, T_2, T_3. These results were calculated with CVM.

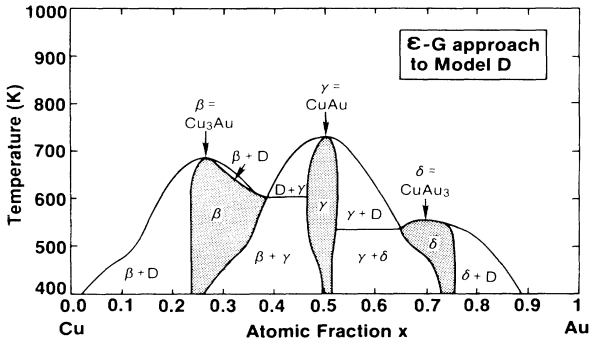

FIG. 20. Calculated phase diagram of Cu-Au in the ε-G approach to model D, using the $\varepsilon^{(n)}$ and $G(X_n)$ values denoted in Table X as "interpolation." Note the great resemblance to the phase diagram of Fig. 13 calculated for model D using the present equation of state approach.

of the important features of a phase diagram, and many of the single-phase phenomena, such as short-range order, are solely determined by the chemical energies $\varepsilon^{(n)}$. From Table X one sees that, whatever the scheme, these energies are calculated with a precision already better than most of the enthalpy measurements. The chemical energies $\varepsilon^{(n)}$ are obtained from Eq. (A7) by integrating $G(x)$ as in Eq. (A6). In the process of integration, the differences between the many $Z(x)$ curves of Fig. 19 are much attenuated. Using $Z(x)$ obtained by interpolation of $\{V^{(n)},B^{(n)}\}$ (Fig. 19, solid curve) and the corresponding interpolated $\varepsilon^{(n)}$ values (Table X), we have performed a CVM calculation of the phase diagram. The results are shown in Fig. 20. We find excellent agreement with the direct equation-of-state CVM approach (Fig. 13).

On the other hand, some thermodynamic potentials depend not on $G(x)$ but on its derivative. For instance, the chemical potential μ has a term

$$\frac{dG}{dx}=\int_x^1(1-x')\frac{B(x')}{V(x')}\left[\frac{dV}{dx'}\right]^2dx'$$

$$-\int_0^x x'\frac{B(x')}{V(x')}\left[\frac{dV}{dx'}\right]^2dx' \qquad \text{(A10)}$$

for which the differences between the many $Z(x)$ become more important. Finally, spinodals which are determined by equating the second derivative of the free energy to zero, depend on $d^2G/dx^2=-Z(x)$ itself. In this case, the spinodal curve will depend on which of the different $Z(x)$ curves is being used.

This analysis shows that the (ε,G) separation will always be very good as a parametrization scheme. On the other hand, when it comes to the calculation of $Z(x)$ by interpolating the sets $\{V_n\}$ and $\{B_n\}$, the results are going to be good for $\varepsilon^{(n)}$, worse for μ [when the first derivative of $G(x)$ intervenes], and even worse for the spinodals and miscibility gaps (when the second derivative intervenes).

[1]R. Hultgren, R. D. Desai, D. T. Hawkins, H. G. Gleiser, and K. K. Kelley, *Selected Values of the Thermodynamic Properties of Binary Alloys* (American Society for Metals, Cleveland, 1973).

[2]K. Terakura, T. Oguchi, T. Mohri, and K. Watanabe, Phys. Rev. B **35**, 2169 (1987).

[3]R. E. Watson, J. W. Davenport, and M. Weinert, Phys. Rev. B **35**, 508 (1987); **34**, 8421 (1986).

[4]D. Gray and E. Brown, Phys. Rev. **160**, 567 (1967).

[5]H. L. Skriver and H. P. Lengkeek, Phys. Rev. B **19**, 900 (1979).

[6]R. E. Watson and L. H. Bennett, Phys. Rev. B **18**, 6439 (1978).

[7]J. A. Alonso and L. A. Girifalco, Phys. Rev. B **19**, 3889 (1979); C. H. Hodges and M. J. Scott, Philos. Mag. **26**, 375 (1972).

[8]J. A. Clark and P. G. Dawber, J. Phys. F **2**, 930 (1972).

[9]C. D. Gelatt and H. Ehrenreich, Phys. Rev. B **10**, 398 (1974).

[10]K. Levin and H. Ehrenreich, Phys. Rev. B **3**, 4172 (1971).

[11]H. Ebert, P. Weinberger, and H. J. Voitländer, Z. Phys. B **63**, 299 (1986).

[12]R. C. Kittler and L. M. Falicov, Phys. Rev. B **18**, 2506 (1978); in *Theory of Alloy Phase Formation*, edited by L. H. Bennett (The Metallurgical Society, Warrendale, PA, 1980), pp. 303.

[13]C. Domb, in *Phase Transitions and Critical Phenomena*, edited by C. Domb and H. S. Green (Academic, London, 1974), Vol. 3, pp. 357.

[14]D. M. Burley, in *Phase Transitions and Critical Phenomena*, edited by C. Domb and M. S. Green (Academic, London, 1972), Vol. 2, p. 329.

[15]R. Kikuchi, J. M. Sanchez, D. de Fontain, and H. Yamaguchi, Acta Metall. **28**, 651 (1980).

[16]R. Kikuchi and J. W. Cahn, Acta Metall. **21**, 1337 (1979).

[17]D. De Fontaine, in *Solid State Physics*, edited H. Ehrenreich, F. Seitz, and D. Turnbull (Academic, New York, 1979), Vol. 37, p. 73.

[18]J. Hijmans and J. De Boer, Physica (Utrecht) **21**, 471 (1955); **21**, 485 (1955); **21**, 499 (1985).

[19]C. M. van Baal, Physica (Utrecht) **64**, 571 (1973).

[20]D. F. Styer, M. K. Phani, and J. Lebowitz, Phys. Rev. B **34**, 3361 (1986).

[21]K. Binder, Phys. Rev. Lett. **45**, 811 (1980).

[22]U. Gahn, J. Phys. Chem. Solids **47**, 1153 (1986).

[23]See, for example, Ya. G. Sinai, *Theory of Phase Transitions: Rigorous Results* (Pergamon, Oxford, 1982).

[24]G. P. Srivastava, J. L. Martins, and A. Zunger, Phys. Rev. B **31**, 2561 (1985). See also J. W. D. Connolly and A. R. Williams, Phys. Rev. B **27**, 5169 (1983) for a closely related approach.

[25]A. A. Mbaye, L. G. Ferreira, and A. Zunger, Phys. Rev. Lett. **58**, 49 (1987).

[26]L. G. Ferreira, A. A. Mbaye, and A. Zunger, Phys. Rev. B **35**, 6475 (1987), and unpublished.

[27]A. G. Khachaturyan, *Theory of Structural Transformations in Solids* (Wiley, New York, 1983).

[28]E. A. Guggenheim, *Mixtures* (Clarendon, Oxford, 1959).

[29]S.-H. Wei, H. Krakauer, and M. Weinert, Phys. Rev. B **32**,

7792 (1985), and references therein.
[30]P. Hohenberg and W. Kohn, Phys. Rev. **136**, B864 (1964); W. Kohn and L. J. Sham, Phys. Rev. **140**, A1133 (1965).
[31]E. Wigner, Phys. Rev. **46**, 1002 (1934).
[32]D. J. Chadi and M. L. Cohen, Phys. Rev. B **8**, 5747 (1973).
[33]F. D. Murnaghan, Proc. Nat. Acad. Sci. **30**, 244 (1944).
[34]A. R. Williams, J. Kübler, and C. D. Gelatt, Jr., Phys. Rev. B **19**, 6094 (1979).
[35]V. L. Moruzzi, J. F. Janak, and A. R. Williams, *Calculated Electronic Properties of Metals* (Pergamon, New York, 1978).
[36]L. Hedin and B. I. Lundqvist, J. Phys. C **27**, 1853 (1984).
[37]M. H. Kang, R. C. Tatar, E. J. Mele, and P. Soven, Phys. Rev. B **35**, 5457 (1987).
[38]J. P. Perdew and A. Zunger, Phys. Rev. B **23**, 5048 (1981).
[39]U. von Barth and L. Hedin, J. Phys. C **5**, 1629 (1972).
[40]D. S. Eppelsheimer and R. R. Penman, Physica **16**, 792 (1950). See more discussion in Vol. 6 of *Landolt-Börnstein, New Series* (Springer-Verlag, Berlin, 1971), p. 7.
[41]Y. Hiki and A. V. Granato, Phys. Rev. **144**, 411 (1966).
[42]C. Kittel, *Solid State Physics,* 5th ed. (Wiley, New York, 1976), p. 74.
[43]J. R. Debesis, Ph.D. thesis, Western Reserve University 1971, quoted in Vol. 11 of *Landolt-Börnstein, New Series* (Springer-Verlag, Berlin, 1979), p. 100.
[44]M. E. Straumanis and S. M. Riad, Trans. AIME **223**, 964 (1965). See more discussion in Vol. 6 of *Landolt-Börnstein, New Series* (Springer-Verlag, Berlin, 1971), p. 1.
[45]R. F. S. Hearmon, Rev. Mod. Phys. **18**, 409 (1946).
[46]P. S. Ho, J. P. Poirier, and A. L. Ruoff, Phys. Stat. Solidi **35**, 1017 (1969).
[47]C. Rolfe, J. Inst. Metals **94**, 148 (1966). See more discussion in Vol. 6 of *Landolt-Börnstein, New Series* (Springer-Verlag, Berlin, 1971), p. 2.
[48]B. Golding, S. C. Moss, and B. L. Averbach, Phys. Rev. **158**, 637 (1967).
[49]P. A. Flinn, G. M. McManus, and J. A. Rayne, J. Phys. Chem. Solids **15**, 189 (1960). See more discussion in Vol. 6 of *Landolt-Börnstein, New Series* (Springer-Verlag, Berlin, 1971), p. 324. The lattice parameter at room temperature, corresponding to the disordered phase, is approximately 3.805 Å; see H. L. Yakel, J. Appl. Phys. **33**, 2439 (1962).
[50]R. Chiarodo, J. Green, I. L. Spain, and P. Bolsaitis, J. Phys. Chem. Solids **33**, 1905 (1972).
[51]C. H. Johansson and J. O. Linde, Ann. Phys. (Leipzig) **25**, 1 (1961); J. B. Newkirk, J. Metals **5**, 823 (1953). See more discussion in Vol. 6 of *Landolt-Börnstein, New Series* (Springer-Verlag, Berlin, 1971), p. 323.
[52]P. Wright and K. F. Goddard, Acta Metal. **7**, 757 (1959). See more discussion in Vol. 6 of *Landolt-Börnstein, New Series* (Springer-Verlag, Berlin, 1971), p. 323.
[53]S. Froyen and C. Herring, J. Appl. Phys. **52**, 7165 (1981).
[54]A. R. Williams, C. D. Gelatt, Jr., and J. F. Janak, in *Theory of Alloy Phase Formation,* edited by L. H. Bennett (The Metallurgical Society, Warrendale, PA, 1980), pp. 40–62.
[55]C. D. Gelatt, Jr., H. Ehrenreich, and R. E. Watson, Phys. Rev. B **15**, 1613 (1977).
[56]A. R. Miedema, P. F. de Châtel, and F. R. de Boer, Physica **100B**, 1 (1980).
[57]M. O. Robbins and L. M. Falicov, Phys. Rev. B **29**, 1333 (1984).
[58]D. Pettifor, J. Phys. F **7**, 613 (1977); J. Friedel, in *Physics of Metals,* edited by J. M. Ziman (Cambridge University Press, Cambridge, 1969), Vol. I, pp. 361–364.
[59]A. R. Williams, C. D. Gelatt, Jr., and V. L. Moruzzi, Phys. Rev. Lett. **44**, 429 (1980).
[60]For a discussion see *Theory of Alloy Phase Formation,* edited by L. H. Bennett (The Metallurgical Society, Warrendale, PA, 1980).
[61]R. E. Watson and L. H. Bennett, in *Theory of Alloy Phase Formation,* Ref. 60, pp. 425–450.
[62]L. Pauling, *The Nature of the Chemical Bond* (Cornell University, Ithaca, NY, 1960).
[63]S. M. Foiles, M. I. Baskes, and M. S. Daw, Phys. Rev. B **33**, 7983 (1986).
[64]Notice that at a fixed composition $V_{\rm eq}^{(n)}(x)$ is a constant, that is $\partial V_{\rm eq}^{(n)}(x)/\partial V\,|_x = 0$.
[65]W. L. Bragg, Philos. Mag. **40**, 169 (1920).
[66]H. L. Yakel, J. Appl. Phys. **33**, 2439 (1962) (the sample used was slightly nonstoichiometric).
[67]L. Topor and O. J. Kleppa, Metallurgical Trans. **15A**, 2 (1984); O. J. Kleppa and L. Topor, in *Nobel Metal Alloys,* edited by T. B. Massalski, W. B. Pearson, L. H. Bennett, and Y. A. Chang (The Metallurgical Society, Warrendale, PA, 1986), pp. 199.